Constraints on VCG Model from GW Merger Events

Astrophysics- B2

Supervisor: **Dr. Geetanjali Sethi**

What we know is a drop, what we don't know is an ocean.

Isaac Newton

Team Members

1. †§Ashley Chraya, Department of Physics, Indian Institute of Science Education and Research (IISER), Mohali

2. §†Yuvraj Muralichandran, Department of Physics (Self Financed Stream), Madras Christian College, Tamil Nadu, India

3. †§Nilkantha Namdev Gholap

4. †R. Jothika, Department of Physics, Amrita Vishwa Vidyapeetham, Coimbatore

5. †Survi Kumari, Department of Physics, Shaheed Rajguru, University of Delhi

---

† Theoretical and Mathematical Analysis
§ Data Collection and Coding

Acknowledgements

We thank Dr. Geetanjali Sethi for accepting to be our supervisor and for suggesting us this topic in which we have developed a deep interest. Our gratitude is not only limited to her scientific experience that guided us towards the research project, but also includes insightful and valuable discussions, we had during our internship duration. We also express our deepest gratitude to her for her patience, continuous support, and for giving us the freedom to learn at our own pace.

Lastly, we would like to thank SARSTEM for generously sponsoring the project

Abstract

Most of the time, the observations have the power to push the well-established field to its most stringent tests. One such observation was of the supernovae type-Ia. There are myriad number of cosmological models explaining this expansion of the universe. One such model is Variable Chaplygin gas model. The variable Chaplygin gas interpolates from dust-dominated era to quintessence dominated era. The model is found to be compatible with current type Ia Supernovae data. In this report, we constrain the parameters of the variable Chaplygin gas model, Ω_m and n, using supernova events and gravitational wave events at different redshifts.

Contents

List of Figures

Introduction

1.1 | Motivation

It is most often that the observations have the power to push the well established field to its most stringent tests. One such observation was of the supernovae type-Ia (SNe-Ia) which established that the universe is expanding. Inference of this observation from the best fit was the value of cosmological constant density parameter to be around 0.7. These results were followed by massive experimental efforts to find other independent observational means to test the expansion of the universe theory. After SNe-Ia observation, there has been number of other such observations which establishes that the expansion is accelerating such as Baryon Acoustic Oscillations (BAO), Cosmic Microwave Background Radiation (CMBR), Gamma-ray Bursts (GRBs). The observational results of SN Ia together with the anisotropy of cosmic microwave background radiation (CMBR) power spectrum and clustering estimates show that our universe is mainly made up of two components: dark matter and dark energy. The dark matter contribute 25% of the total energy density of the universe whereas dark energy contributes 70% of the total energy density of the universe.

SN observations have been one of the important way to constrain the model in cosmology. SN, along with BAO and CMB observations are now the three major pillars of any analysis. Though there are other ways like Large scale structure surveys, gravitational lensing surveys etc., which all help to constrain parameters of the model. We would not be able to do any justice in this report to discuss these observations in any detail, hence, we would only focus on Supernova type-Ia observations.

In fact, it was in 1920s when Alexander Friedmann and Georges Lemaître independently provided first cosmological model which explained that the universe is expanding. There are many different cosmological models which explain the expanding universe. One such model which is most favourable is ΛCDM model (Lambda cold dark matter) where Λ is the cosmological constant. This model is referred to as the standard model of Big Bang cosmology. This standard model of cosmology explains a lot of observations. The cosmological constant in general relativity combined with the assumed homogeneous and isotropic FRW metric description of spacetime gives us ΛCDM model. Λ refers to the cosmological constant which is commonly known as dark energy (a force that repels gravity). CDM is the cold dark matter where dark is

because we can't see it, and cold is because it behaves like non-relativistic particles compared to massless particles, for example neutrinos, which are relativistic particles, hence, hot. As dark matter and dark energy together contributes to around 95% of matter in the universe, the remaining 5% are Baryonic matter i.e. all the particles of the standard model of particle physics, not just Baryons. In spite of this model to explain many observations, it suffers from fine tuning problem. Hence, there are many cosmological models which remains active areas of research in cosmology today and they all involve trying to understand the nature of dark matter and dark energy. Different models explored can be broadly categorized into two classes. One class of models involve reforming the geometry part of the Einstein's equations. This includes generalisation of gravity action and higher dimension spacetime. The other class of models alter the matter component of the Universe in the Einstein's equations. In this approach exotic matter with negative pressure is added to the mass distribution of the Universe. Some of the models based on this are quintessence, k-essence, tachyons, barotropic fluid etc. These are collectively known as Dark Energy models. Recently, an alternative class of models have been proposed which involve a slowly evolving and spatially homogenous scalar field or two coupled fields. However, these "Quintessence" models also suffer from fine tuning problem. Quintessence, k-essence are scalar field models, while Dark Energy models include barotropic fluids whose pressure is a function of energy density, $P = f(\rho)$. The relationship between pressure and energy density determines the dynamics of the fluid. One such example of a barotropic fluid is the Chaplygin gas, which will be our main focus in this report.

Bringing pieces together, we will try to explain how to put constraints on the parameters of the Variable Chaplygin gas model using supernova events and gravitational wave merger events. In chapter 2, we give brief review of the basic cosmology topics like FLRW, Freidmann equations etc., Λ CDM model, Variable Chaplygin gas model. In chapter 3, we review how Supernova and gravitational wave merger events can be used to measure cosmological distances. In chapter 4, we discuss supernova and gravitational wave datasets which we use to constrain the cosmological model. In chapter 5, we discuss usages of some packages in gravitational wave data analysis. In chapter 6, we discuss the statistical tool we use to constrain the model. In chapter 7, we constrain the parameters of the Variable Chaplygin gas model using Chi-square minimization method and discuss our results obtained using both SN and GW merger events. Finally, in chapter 8, we discuss what lies further for us to work on in this domain.

1.2 | Scope of this report in a nutshell

The absolute scope of this project is to find the performance of a novel cosmological model i.e. Variable Chaplygin gas model with an new branch of astrophysics i.e. gravitational wave astronomy. The project will pave a way to test if gravitational waves can be used as a new

independent way to constrain cosmological models. The project will also provide us an understanding if gravitational wave merger events can be used to obtain Hubble constant as an independent test from cosmic distance ladder. Meanwhile comparing the performance of Variable Chaplygin gas in both supernovae dataset and Gravitational Waves merger event dataset helps us to calibrate our current understanding on the universe.

Cosmology: Basics

2.1 | The FLRW metric

Friedmann–Lemaître–Robertson–Walker (FLRW) metric is the solution of the Einstein's equation assuming space is homogeneous and isotropic. The general form of the metric can be derived from homogeneity and isotropy of the space. We will derive it step by step below:
Firstly, we note that the general metric can be written as

$$ds^2 = g_{\alpha\beta}dx^\alpha dx^\beta$$
$$= g_{00}dt^2 + 2g_{0i}dx_{ij} - h_{ij}dx^i dx^j \tag{2.1}$$

where i,j runs as $1, 2, 3$ and h_{ij} is the spatial metric.
(1) Assuming isotropy of the space i.e. we can transform spatial coordinates as $x \to -x$, and the equation of motions should not change i.e. metric remains same. We can easily conclude from the transformation that $g_{0i} = 0$. Therefore, the metric can be written as

$$ds^2 = g_{00}dt^2 - h_{ij}dx^i dx^j \tag{2.2}$$

(2) Using the transformation $d\tau = \sqrt{g_{00}}dt$, we can write the metric as (writing t instead of τ)

$$ds^2 = dt^2 - h_{ij}dx^i dx^j \tag{2.3}$$

(3) Due to isotropy the space should be spherically symmetric therefore, the spatial metric can be written in cartesian coordinates as

$$d\Sigma^2 = h_{ij}dx^i dx^j = dx^2 + dy^2 + dz^2 \tag{2.4}$$

as all mixed terms dxdy, dydz etc vanishes due to isotropy. Now considering spherical coordinate system, h_{ij} should only be dependent on r and t i.e., $h_{ij}(r, t)$ (h_{ij} can be dependent on time as the symmetries are only applied at t=constant hypersurface) and shouldn't be dependent on angles i.e., θ and ϕ. Further, we assume that this function is separable i.e. $h_{ij}(r, t) = a(t)\lambda(r)$. Therefore, the spatial metric becomes

$$d\Sigma^2 = a(t)^2\lambda(r)^2[dr^2 + r^2(d\theta^2 + \sin^2\theta d\phi^2)] \tag{2.5}$$

Taking $\lambda r = r'$ and redefining $\lambda' = \frac{\lambda}{r\frac{d\lambda}{dr}+\lambda}$, we get

$$d\Sigma^2 = a^2[\lambda'^2 dr'^2 + r'^2(d\theta^2 + \sin\theta d\phi^2)] \tag{2.6}$$

Till now we have imposed isotropy, but now we will impose homogenity further to get the expression for $\lambda'^{(r)}$. We now seek the metric that describes a hypersurface immersed in a spherical four-dimensional Euclidean space. The properties of this hypersurface will obviously be the same for every point belonging to it due to homogenity. Therefore the above spatial metric obtained will be equivalent to the metric which we will derive now of a 3D sphere. For a 3D sphere we know,

$$a^2 = x_1^2 + x_2^2 + x_3^2 + x_4^2 \tag{2.7}$$

where a is fixed. Using 4- dimensional spherical coordinates,

$$\begin{aligned}
x_1 &= a\cos\chi\sin\theta\sin\phi \\
x_2 &= a\cos\chi\cos\theta \\
x_3 &= a\cos\chi\sin\theta\cos\phi \\
x_4 &= a\sin\chi
\end{aligned} \tag{2.8}$$

Differentiating 2.7, and using it in $ds^2 = dx_1^2 + dx_2^2 + dx_3^2 + dx_4^2$ we get

$$ds^2 = a^2\left(d\chi^2 + \sin^2\chi\left(d\theta^2 + \sin^2\theta d\phi^2\right)\right) \tag{2.9}$$

As this metric should be equivalent to 2.6, we conclude $\sin\chi = r$ and $d\chi = \lambda dr$ i.e.

$$\lambda = \frac{1}{\sqrt{1-r^2}} \tag{2.10}$$

Now, generalizing the line element

$$a^2 = x_1^2 + x_2^2 + x_3^2 + kx_4^2 \tag{2.11}$$

This line element is homogeneous as it was in the previous spherical case. Now, proceeding as before, we obtain

$$ds_3^2 = a^2\left(d\chi^2 + F(\chi)\left(d\theta^2 + \sin^2\theta d\phi^2\right)\right) \tag{2.12}$$

where

$$F(\chi) = \begin{array}{ll}
\sin\chi & k = 1 \\
\chi & k = 0 \\
\sinh\chi & k = -1
\end{array} \tag{2.13}$$

and

$$\lambda = \frac{1}{\sqrt{1-kr^2}} \tag{2.14}$$

Therefore, in conclusion, the homogeneous and isotropic metric obtained which is known as FLRW metric is

$$ds^2 = dt^2 - a^2(t) \left[\frac{dr^2}{1 - kr^2} + r^2 \left(d\theta^2 + \sin^2\theta d\phi^2 \right) \right] \tag{2.15}$$

where k can take values $k = 0, \pm 1$. As we have seen that to derive the expression for $\lambda(r)$, we needed homogenity of space, but to derive the expression for scale factor $a(t)$, we will need Einstein's field equations. This model is sometimes called the Standard Model of modern cosmology, although Lambda-CDM model is also often called called the Standard Model of modern cosmology. The FLRW metric was independently derived by the authors in the name of FLRW in 1920s and 1930s.

2.1.1 | Co-moving Coordinate v/s Physical Distance

Co-moving coordinates expand with universe at the same rate as the universe, hence, distance between any two objects calculated in this coordinate also remains same. Therefore, co-moving distance remains same between any two observers at any epoch. In FLRW metric in spherical coordinates, the spatial coordinate dr is the co-moving coordinate.

On the other hand, physical distance as we know changes as the objects move away due to expansion of the universe from each other. We can relate the physical distance and co-moving distance as follows:

Assuming FLRW metric and light travelling the null geodesic (taking c=1), we obtain,

$$dt^2 = a^2(t) \left[\frac{dr^2}{1 - kr^2} + r^2 \left(d\theta^2 + \sin^2\theta d\phi^2 \right) \right] \tag{2.16}$$

Also assuming $d\theta$=dϕ=0, we get,

$$cdt = \frac{adr}{\sqrt{1 - kr^2}} \tag{2.17}$$

Further, if we assume light travelling a small distance, we obtain the relation,

$$cdt = a(t)dr \tag{2.18}$$

We should notice that this relation is valid only for small distance in general but for flat space k=0, this relation is universally valid.

Here, r is the comoving distance which is fixed on space and time and "move" with it. The physical distances $D = a(t)r$ vary instead with the expansion. For convenience, we often define the present distances such that D = r, i.e. $a(t = 0) = 1$. In this way, the astronomical distances measured at the present epoch, for example, the distance between the Milky Way and the Virgo Cluster, are also comoving distances, which are fixed forever. In other words, the comoving distance of the Virgo cluster is 15 Mpc at every epoch.

2.1.2 | Hubble's Law

Hubble's law is the observation that galaxies are moving away from Earth at speeds proportional to their distance. The farther they are the faster they are moving away from Earth. This observation can be derived from FLRW metric as follows: The physical distance measured along a null geodesic $ds = 0$ for a small propagation and considering $d\theta = d\phi = 0$, is $D = cdt = a(t)dr$. Thereofre, we have the Hubble's law

$$\dot{D} = \dot{a}dr = HD \tag{2.19}$$

where $H = \frac{\dot{a}}{a}$ is the Hubble constant. Hubble's law applies to any system that expands (or contracts) in a homogeneous and isotropic way, and it is valid only for small distances. For flat space, it is valid at any distance scale.

2.1.3 | Redshift

Consider a wave source at rest. The interval between two crests is $dt = \frac{\lambda_{em}}{c}$ where λ_{em} is the wavelength of the emitted source and c is the speed of the light. If now in the same time interval dt, the source moves away from the observer at velocity v, then the distance travelled by the source is vdt and therefore, the observed wavelength is $\lambda_{ob} = cdt + vdt$. Thus there is a difference between emitted wavelength and observed wavelength (doppler effect).

$$\frac{d\lambda}{\lambda} = \frac{\lambda_{obs} - \lambda_{em}}{\lambda_{em}} = \frac{v}{c} \tag{2.20}$$

The redshift is defined as

$$z \equiv \frac{\lambda_{\text{obs}} - \lambda_{\text{em}}}{\lambda_{\text{em}}} \tag{2.21}$$

If the source is following Hubble's law $\dot{D} = v = HD$ from which we obtain

$$\frac{d\lambda}{\lambda} = \frac{v}{c} = \frac{HD}{c} = Hdt = \frac{da}{a} \tag{2.22}$$

Taking integeration from emitted time to observed time, and normalizing the scale factor such that at the present epoch $a = a_0 = 1$, we obtain $\frac{\lambda_{ob}}{\lambda_{em}} = a_{em}$. Using this we can obtain an important relation which relates easily calculable redshift with the cosmological function a(t):

$$a = \frac{1}{1+z} \tag{2.23}$$

The above equation is valid only for small distances as we have assumed source follows Hubble's law which is followed only for small distance propagation. Also we have assumed here that in dt time source moves a distance of vdt taking non-relativistic kinematics into account. Therefore, if we assume relativistic version or if the source is moving at relativistic speed (at large distance v≪c is no longer valid) the above relation will not be valid.

2.2 | Energy-Momentum Tensor and Energy Conditions

We can define energy-momentum tensor as:

$$T^{\alpha\beta} = (p + \rho)U^\alpha U^\beta - pg^{\alpha\beta} \tag{2.24}$$

In the rest frame $U^\alpha = (1,0,0,0)$, $T^{\alpha\beta}$ can be written as

$$T^{\nu\mu} = \text{diag}(\rho, -p, -p, -p) \tag{2.25}$$

Conservation of energy momentum tensor is

$$T^{\mu\nu}_{,\mu} = 0 \tag{2.26}$$

2.2.1 | Continuity Equation and Conservation of scalar quantity

Below, we will show by two methods how continuity equation implies conservation of the concerned quantity. Assuming, the continuity equation,

$$\partial_k J^k = 0 \tag{2.27}$$

Now, by using Gauss theorem,

$$\int_\Omega d^4V \left(\partial_\mu J^\mu \right) = \oint_{\partial\Omega} dS \left(J^\mu n_\mu \right) \tag{2.28}$$

where n_μ is the normal of the boundary surface. Assuming the boundary to be a cylinder as shown in the figure below, and assuming the concerned quantity vanishes at spatial infinity, we can show the conservation of the quantity.
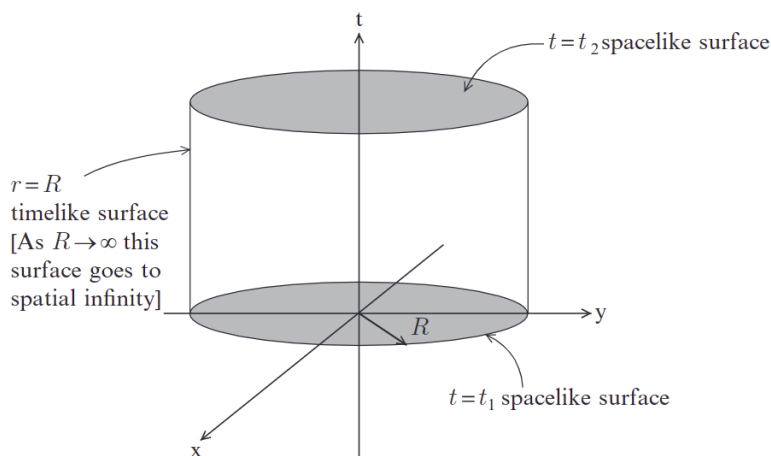
Figure 2.1: The Gauss theorem in a spacetime volume is illustrated

There is another intiutive way to show that continuity equation implies conservation of scalar quantity. Assume a box in the spacetime, through the faces of which current is flowing. If we consider the face of the box in the yz plane then we can conclude that current flowing through the box in x direction is $-\partial_x j_x$, similarly for the other faces of the box we can show the similar result. Hence, the total current passing through the box is $-\nabla.\vec{J}$ which should be equation to the total change in the quantity in the box $\frac{\partial \rho}{\partial t}$, hence

$$\frac{\partial \rho}{\partial t} + \nabla.\vec{J} = 0 \tag{2.29}$$

2.2.2 | Energy-Momentum Tensor Conservation and Continuity equation

Taking conservation of stress energy tensor, $\nabla_\mu T^{\mu\nu} = 0$, and substituting $T^{\mu\nu} = (\rho + p)(U^\mu U^\nu) + p g^{\mu\nu}$, and project the equation on different directions to get the 2 equations:

$$U^\mu \partial_\mu \rho = -(\rho + p)\nabla_\mu U^\mu \tag{2.30}$$

$$(\rho + p)U^\mu \nabla_\mu U_\nu = -\nabla_\nu p - U_\nu U^\mu \nabla_\mu p \tag{2.31}$$

The first equation is a conservation equation ρ, and the second is a conservation equation for the momentum.

We can also obtain the former equation by taking time component of the energy momentum tensor conservation 2.26. This equation is referred to as continuity equation.

$$\frac{\partial \rho}{\partial t} + 3H(p + \rho) = 0 \tag{2.32}$$

Note: Continuity equation remains invariant under the addition of constant to the Lagrangian of gravitational action.

2.2.3 | Dust, Ideal Fluid and Radiation

Dust is a pressure-less fluid which has an exact solution to Einstein's field equation whose energy momentum tensor can be written as

$$T_{ab} = \rho U_a U_b \tag{2.33}$$

where U_a is the 4-velocity of the dust and ρ is the energy density of the dust. In contrast to pressure-less dust, ideal fluid also has an exact solution to Einstein's field equation whose energy momentum density can be written as

$$T_{ab} = (\rho + p)U_a U_b - p g_{ab} \tag{2.34}$$

$$T_b^a = (\rho + p)U^a U_b - p\delta_b^a = \rho U^a U_b - p(\delta_b^a - U^a U_b) \tag{2.35}$$

where $P_b^a = \delta_b^a - U^a U_b$ is the Projection tensor as it is symmetric and $P_b^a U^a = 0$ perpendicular to 4-velocity vector i.e. all the 4- vectors perpendicular to U^a can be obtained. Therefore, for ideal fluid

$$T_b^a = \rho U^a U_b - p P_b^a \tag{2.36}$$

We know that for radiation equation of state reads as,

$$p = \frac{\rho}{3} \tag{2.37}$$

Using the above equation and taking the trace of the equation, 2.36, we get $T_a^a = 0$. Therefore, trace of energy momentum tensor for radiation vanishes. This vanishing of energy momentum tensor is a general feature of any electromagnetic field which is explored below.

2.3 | Modified gravity and Cosmological models

In 1920s, Alexander Friedmann theorized that the Universe is expanding using Einstein field equations after Vesto Slipher identified redshift of many galaxies. This theory was proved by the observational evidences from Edwin Hubble. George Lemaitre provided the linear relation between the distance of the galaxy and the redshift observed in them due to expansion of the universe.

In early 1990s, with the observations of type Ia Supernovae (SNe-Ia) by independent research groups Supernova Cosmology Project (SCP) and the High-Z Supernova Search, the expansion of the universe was found to be accelerated compared to the initial assumption of the linear expansion by George Lemaitre. By the Friedmann-Robertson-Walker metric of the Universe, the expansion is directly proportional to the amount of matter present in the Universe. With accelerated expansion, the universe needed additional presence of mass or energy to be explained with the current cosmological model. With no evidence on these additional matter from Electromagnetic Radiations, this additional energy was termed as Dark Energy.

Similarly in 1930s, Fritz Zwicky found in the Coma cluster that mass of the galaxies has to be higher than the visible matter to validate the higher orbital speed of the periphery of the galaxies. He proposed a presence of electromagnetically "dark matter" causing such anomalous high speed of rotations. This was proved by observations of Vera Rubin and others in 1970s and the theory of Dark Matter came into consideration.

The pressing need to explain such phenomenon resulted in theorizing different models which clubbed in these exotic entities in them. All different models can be categorized into two classes. One class of models try to modify the geometry part of the Einstein's equation i.e. Einstein tensor G_{ij}. These theories are known as modified gravity. Einstein-Hilbert action is

$$A_g = \frac{-1}{16\pi k} \int R\sqrt{-g}d^4x \tag{2.38}$$

In modified gravity, action is written as

$$A_{mg} = \frac{-1}{16\pi k} \int f(R)\sqrt{-g}d^4x \qquad (2.39)$$

where $f(R)$ is a function of Ricci scalar,A_g is the action for GR, A_{mg} is the action for modified gravity. One also work in higher dimensions instead of four as a part of modifying gravity.

As due to observations, it was not possible to explain the accelerated universe if only normal matter is taken into consideration. Hence, exotic matter i.e. dark matter has to be added to the energy momentum tensor. The other class of models assumes universe is governed by general relativity but alter the matter component of the Einstein's equation i.e. Energy-Momentum tensor T_{ij}. Models in both classes explain the expanding universe. The presence of these exotic entities are brought in the ΛCDM (Λ Cold Dark Matter) model. Models based on this dark matter can be further divided into quintessence models and barotropic fluids. In quintessence models slowly evolving and spatially homogeneous scalar field or two coupled fields are considered. It differs from cosmological constant explanation of expansion of universe in the sense that cosmological constant is constant over time whereas in this model time varying scalar field is assumed. Quintessence models also suffer from fine tuning problem, therefore, possible alternative which we should look into is dark energy models like barotropic fluids. Therefore, we now know that observations show that exotic matters like dark energy and dark matter are required to explain the acceleration of the universe, below we express the energy momentum tensor of dark energy in comparison to other matter.

2.4 | Chaplygin Gas Model

Dark energy models including barotropic fluids have pressure as a function of energy density, $P = f(\rho)$, which determines the dynamics of the fluid. These models also contains classes with varying equation of state. One specific example of the barotropic fluid is Chaplygin gas (CG) whose equation of state is $P = -A/\rho$, where A is a positive constant. Chaplygin gas model correctly describes the effects of dark energy and dark matter, and is a alternate for our current standard model of cosmology. As described in the previous section dark energy models have negative pressure, CG model also has a negative pressure associated with it and the more generalized model of CG is described by the equation of the sate given as

$$p = -\frac{A}{\rho^\alpha} \qquad (2.40)$$

where p is the pressure, ρ is the energy density, both in a comoving reference frame with $\rho > 0$, A and α ($0 < \alpha \leq 1$) are positive constants ($\alpha = 1$ corresponds to CG). In FLRW metric, energy

conservation equation is given by

$$\dot{\rho}_i + \frac{3\dot{a}}{a}(p_i + \rho_i) = 0 \tag{2.41}$$

This is the fluid equation which holds for radiation(r), Baryonic matter(b) and chaplygin gas(ch), i.e. $i = r, b, ch$. In this report, we assume the universe is filled with CG-radiation-baryonic matter. Using 2.40 and 2.41, we can get the expression for the energy density of the CG given by

$$\rho_{ch} = \left(A + \frac{B}{a^{3(1+\alpha)}}\right)^{\frac{1}{1+\alpha}} \tag{2.42}$$

where B is the constant of integration and a is the scale factor. Hence, we got the equation of state and energy density of the CG model given by 2.40 and 2.42 respectively. We can similarly find the energy density for baryonic matter and radiation given their equation of state. Equation of state for baryonic matter is $p = 0$. Using energy conservation equation 2.41 we can obtain the energy density of the baryonic matter given by

$$\rho_b = \rho_{b0}a^{-3} \tag{2.43}$$

where ρ_{b0} is the integration constant. Equation of state for the radiation is $p = \rho/3$. Radiation is the ideal fluid, hence, energy momentum tensor in curved spacetime can be written as $T^i_j = (p + \rho)U^i U_j - pg^i_j$. Taking trace of this equation we get $T^i_j = p + \rho - 4p = \rho - 3p$. Using equation of state we get the trace of the energy momentum tensor for the radiation to vanish. This vanishing of trace of T_{Ij} is a common feature for theories which are conformally invariant. Anyways, repeating the same story which we did for CG and baryonic matter i.e using energy conservation equation 2.41, we can obtain the energy density of the radiation which is given by

$$\rho_r = \rho_{r0}a^{-4} \tag{2.44}$$

Total energy density can be written as the sum of the components 2.42, 2.43, 2.44, given by

$$\rho_{total}(a) = \left(A + \frac{B}{a^{3(1+\alpha)}}\right)^{\frac{1}{1+\alpha}} + \rho_{b0}a^{-3} + \rho_{r0}a^{-4} \tag{2.45}$$

The Friedmann equation gives the expansion rate of the Universe in terms of matter and radiation density,ρ, curvature,k, and the cosmological constant,Λ, as

$$H^2 \equiv \left(\frac{\dot{a}}{a}\right)^2 = \frac{8\pi G}{3}\rho - \frac{k}{a^2} + \frac{\Lambda}{3} \tag{2.46}$$

where $H \equiv \frac{\dot{a}}{a}$ is the Hubble parameter. Assuming spatially flat universe, we get

$$H^2 = \frac{8\pi G}{3}\rho \tag{2.47}$$

Using total energy density expression 2.45, Freidmann equation 2.46 reads as

$$3H^2 = 8\pi G \left(A + \frac{B}{a^{3(1+\alpha)}} \right)^{\frac{1}{1+\alpha}} + \rho_{b0} a^{-3} + \rho_{r0} a^{-4} \tag{2.48}$$

We can also make change of variables and use redshift, z, instead of using scale factor, a, which is not a physically measurable quantity. The relation between redshift and scale factor is given by

$$1 + z = \frac{a_0}{a} \tag{2.49}$$

where a_0 is the scale factor at the present time which we normalize to 1. Freidmann's equation in terms of redshift can be written as

$$3H^2(z) = \left\{ \left[A + B(1+z)^{3(1+\alpha)} \right]^{\frac{1}{1+\alpha}} + (\rho_{r0}) (1+z)^4 + (\rho_{b0}) (1+z)^3 \right\} \tag{2.50}$$

2.4.1 | Evolution of Chaplygin Gas

We can determine the evolution of the energy density of the CG during different epochs by analyzing equation 2.42. At early times, $a \ll 1$, 2.42 can be written as

$$\rho_{ch} = \frac{B^{1/(1+\alpha)}}{a^3} \tag{2.51}$$

Original CG energy density by using $\alpha = 1$ can be written as

$$\rho_{ch} = \frac{\sqrt{B}}{a^3} \tag{2.52}$$

Therefore, at early times OCG corresponds to dust like matter(or dark matter). On the other hand, at late times we can similarly show that

$$\rho_{ch} = -p = A^{1/(1+\alpha)} = Constant \tag{2.53}$$

Following the discussion in **??**, we can conclude that CG at late times corresponds to a cosmological constant. Thus leads to the observed accelerated expansion. Therefore, we can further conclude that CG evolves from the dust dominated epoch to cosmological constant in present times, and thus CG model can unify CDM and the Λ model features. Therefore, the CG model is a good alternative to explain the accelerated expansion of the universe. However the CG model produces an exponential blowup of matter power spectrums that are inconsistent with observations. Due to this, a modification of the CG model is proposed called Variable Chaplygin Gas model.

2.5 | Variable Chaplygin Gas Model

Equation of state of the Variable Chaplygin Gas (VCG) is given by

$$\rho_{ch} = \frac{A(a)}{p} \tag{2.54}$$

where where p is the pressure, ρ is the energy density, both in a comoving reference frame with $\rho > 0$, $A(a) = A_0 a^{-n}$ is a positive function of the cosmological scale factor a. A_0 and n are constants. Using 2.41, we can find the energy density of VCG as

$$\rho_{ch} = \sqrt{\frac{6}{6-n}\frac{A_0}{a^n} + \frac{B}{a^6}} \tag{2.55}$$

where B is the positive integration constant. For n=0, OGC behaviour is recovered. Assuming universe to be spatially flat, 2nd Freindmann equation can be written as

$$2\frac{\ddot{a}}{a} + H^2 = -\frac{8\pi G}{c^2}p \tag{2.56}$$

The acceleration condition, $\ddot{a}$ can be written as

$$(H^2 + \frac{8\pi G}{c^2}p)a < 0 \tag{2.57}$$

Using equation of state of VCG 2.54 and energy density of VCG 2.55, we find the above acceleration condition is equivalent to

$$3\frac{4-n}{6-n}a^{6-n} > \frac{B}{A_0} \tag{2.58}$$

As both B and A_0 are positive constants, hence $n < 4$. At present time, a=a_0= 1, hence, the present value of the energy density of VCG is given by

$$\rho_{ch0} = \sqrt{\frac{6}{6-n}A_0 + B} \tag{2.59}$$

Defining the parameter, Ω_m,

$$\Omega_m = \frac{B}{6A_0/(6-n) + B} \tag{2.60}$$

the energy density becomes

$$\rho_{ch}(a) = \rho_{ch0}\left[\frac{\Omega_m}{a^6} + \frac{1-\Omega_m}{a^n}\right]^{1/2} \tag{2.61}$$

Total energy density of the universe can be written as the sum of components 2.61, 2.43, 2.44, given by

$$\rho_{total}(a) = \left(\rho_{ch0}\left[\frac{\Omega_m}{a^6} + \frac{1-\Omega_m}{a^n}\right]^{1/2}\right) + \rho_{b0}a^{-3} + \rho_{r0}a^{-4} \tag{2.62}$$

Defining $\Omega_{r0} = \frac{8\pi G \rho_{r0}}{3H_0^2}$ and $\Omega_{b0} = \frac{8\pi G \rho_{b0}}{3H_0^2}$, $\Omega_{ch0} = \frac{8\pi G \rho_{ch0}}{3H_0^2}$ as dimensionless density parameters. The density parameters for radiation and baryonic matter can be expressed as

$$\Omega_r(z) = (\Omega_{r0})(1+z)^4, \quad \Omega_b(z) = (\Omega_{b0})(1+z)^3 \tag{2.63}$$

The total density parameter for a universe where CG, baryonic matter and radiation dominate can be written as

$$1 = \Omega_r(z) + \Omega_b(z) + \Omega_{ch}(z) \tag{2.64}$$

Using total energy density expression 2.62 and 2.49, Freidmann equation 2.46 in terms of redshift reads as

$$H^2 = \Omega_{ch0} H_0^2 (1+z)^4 X^2(z) \tag{2.65}$$

where

$$X^2(z) = \frac{\Omega_{r0}}{1 - \Omega_{r0} - \Omega_{b0}} + \frac{\Omega_{b0}}{1 - \Omega_{r0} - \Omega_{\theta 0}(1+z)} + \frac{\left(\Omega_m(1+z)^6 + (1-\Omega_m)(1+z)^n\right)^{1/2}}{(1+z)^4} \tag{2.66}$$

To test VCG model, the above equation 2.66 is useful. There are two free paramters in the above equation Ω_m and n. We can use the distance modulus,μ, for Supernovae Type IA data and gravitational waves from compact binary coalescence's (CBCs), and calculate the corresponding distance modulus for the CG model at corresponding redshifts.

2.6 | Bibliography Notes

This whole chapter was greatly influenced wide range of sources which are provided in the reference section. The equations are derived from primary work done in Sethi et al. (2018)

3

Standard Candles and Standard Sirens

3.1 | The Distance Ladder

To determine the distance standard candles are used. Standard candles are fictitious objects of constant luminosity for which apparent magnitude is directly related to distance. Distances are measured in a number of ways that are valid for different ranges and different types of sources that rely on previous methods used to measure the distance, such as forming a ladder. Astronomers build what is known as the cosmic distance ladder by combining several ways for determining distances. Objects deemed to be of standard brightness are identified and calibrated in terms of measurements contributing to the preceding rung on each step of the ladder. Thus, methods higher on the rung of the ladder depends on the lower rung to extend the distance range. Thus, to peek further into space where small-scale distance measurement methods are rendered useless, we use methods higher on the rung. Therefore, studying methods to measure small scale distance is an important task. There are currently several sophisticated ways for estimating the Hubble constant, but all of them rely on the distance ladder in some manner.
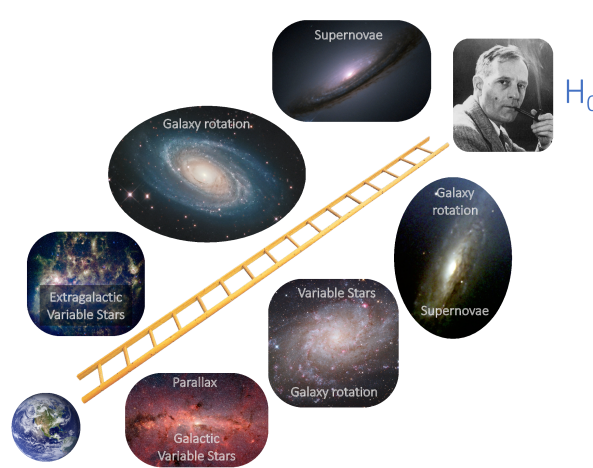

Figure 3.1: The Distance Ladder

3.2 | The Parallax Method

The parallax approach, which is valid up to 50 kpc, i.e. the distance between adjacent satellite galaxies, is one fundamental way for determining distance. This first stage serves as the foundation for all subsequent procedures. When the Earth is at opposing points on the ecliptic (i.e. 2A.U.= 300 million kilometres apart), the goal is to discover the change in direction to a nearby star with regard to the Sun. The star is at infinity if there is no change. Simple trigonometry demonstrates that if the parallax is 1 arcsec, the star is about $2 * 10^1 3$ km distant, i.e. (by definition) 1 parsec= 3.26 light years. The distance in general is then

$$d = \frac{1\text{pc}}{\theta[\text{arcsec}]} \tag{3.1}$$

3.3 | Cepheids

The standard candle (an astronomical source whose inherent brightness is supposed to be known) is an essential instrument for determining distances to objects outside our galaxy. Suppose a star has luminosity L and observers on Earth measure it to have a flux F. From the inverse square law and assuming the star radiates isotropically, we obtain the luminosity distance

$$D = \sqrt{\frac{L}{4\pi F}} \tag{3.2}$$

Nature does not provide observers with stars whose luminosities are precisely known. However, it does provide stars and other objects whose luminosities can be inferred accurately. The second most significant approach is based on Cepheid variable stars. These variable stars are red giants that have reached the end of their lives. When the temperature rises, the He envelope ionises; ionised He is very opaque to radiation from the core, which is trapped and expands the envelope, making the star brighter. The temperature lowers as the envelope expands, and the helium recombines (de-ionizes), making the envelope more transparent. The radiation escapes, the pressure drops, the envelope contracts, and the star dims. The contraction, on the other hand, raises the temperature again, and the cycle begins again, lasting anywhere from a few days to many weeks. For thousands of years, the series of oscillations has been relatively steady. The relation between peak absolute luminosity and period is

$$L \sim P^{1.3} \tag{3.3}$$

By studying a group of such stars in the Small Magellanic Cloud—a dwarf galaxy near the Milky Way—Henrietta Leavitt discovered in 1912 that each star's oscillation period correlates with its intrinsic luminosity. To fix the proportionality constant in this relation (and ensure
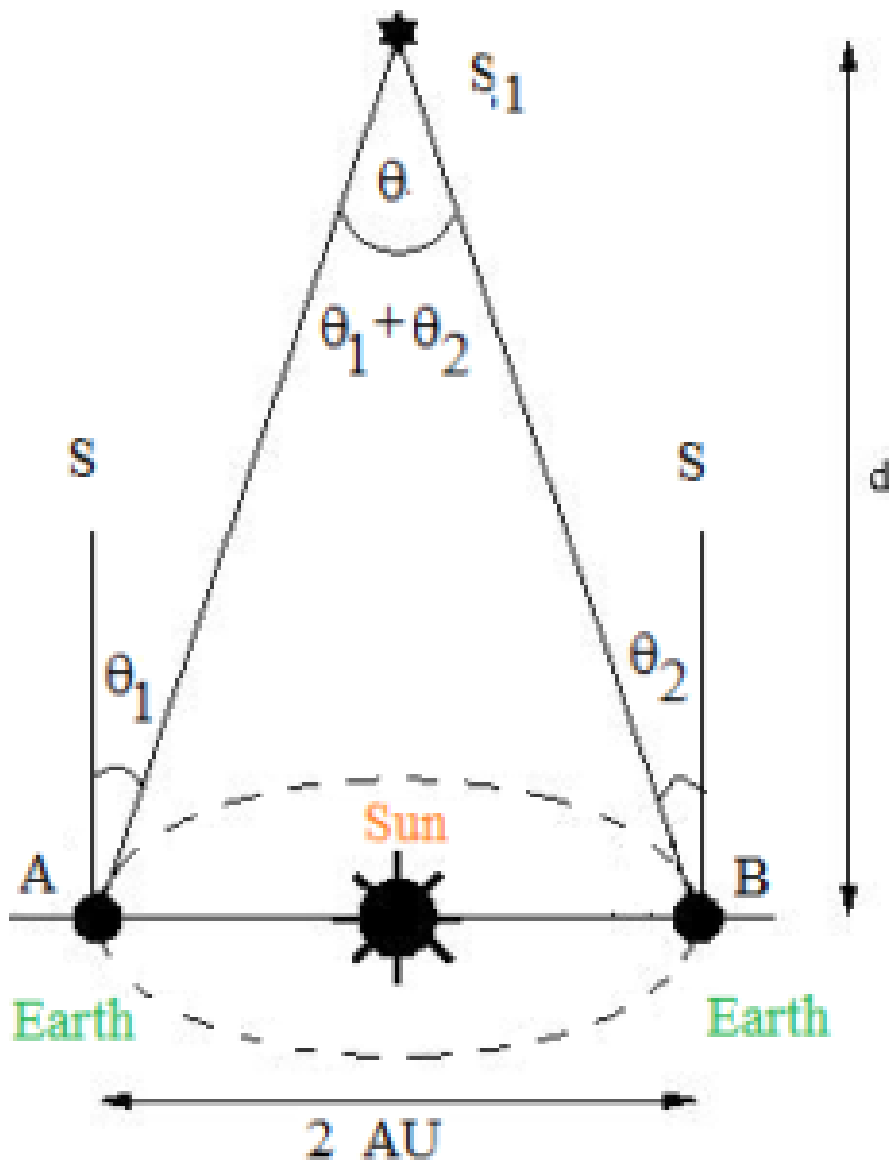
Figure 3.2: The Parallax Method

that it is truly universal, i.e. it applies to all Cepheids), one must calibrate it, which means measuring the luminosity and period for a number of nearby Cepheids for which we know the distance (and thus the absolute magnitude) using the parallax method. This is the most important stage, and it is essential for all other approaches. Cepheid variable stars can serve as standard candles for determining distances beyond the boundaries of parallax after the luminosity–period relation has been empirically established.

3.4 | Supernovae Ia

Supernova is a high-energy phenomena that takes place at the end of stellar evolution. Eventhough the discrete objects in the far away galaxies become faint and hard to resolve, a supernova explosion makes an exception.The consistent luminosity curve and relatively homogeneous properties of a type Ia supernova make it the perfect choice of standard candle for a cosmologist. In 1998 Riess et al. [High-redshift Supernova Search Team (HSST)] and Perlmutter et al. [Supernova Cosmology Project (SCP)] independently reported the late-time cosmic acceleration by observing distant supernovae of type Ia (SN Ia).

Supernova explosions are extraordinarily bright and causes a burst of radiation. Supernovae can be categorised based on chemical element absorption lines. A supernova is categorised as Type II if its spectrum contains a spectral line of hydrogen. Otherwise, it is referred to as Type I. If a supernova has an absorption line of singly-ionized silicon, it is designated as Type Ia (notice that Type Ib has a helium line, but Type Ic lacks both silicon and helium lines). When the mass of a white dwarf in a binary system surpasses the Chandrasekhar limit by absorbing gas from a companion star, a Type Ia explosion occurs.

A white dwarf is a relatively simple object that cools passively by balancing gravity and the electron degeneracy pressure, without undergoing nuclear fusion. When the mass surpasses the limit, the star collapses, but unlike regular stars, the degeneracy pressure cannot rise since it is temperature independent. The temperature rises so quickly that the heavier nuclei (mainly C and O) fuse, and the thermal velocity of the particles surpasses the escape speed, causing the star to burst. The Chandrasekhar limit depends only on fundamental constants, therefore, one expects therefore that the energy emitted by the disruption of such an object is an almost universal constant. This hypothesis must be tested, which may be done using the standard calibration approach, i.e. a sample of nearby SN Ia for which we know the distance via other methods, and from which we can get their absolute magnitude. Then the SN Ia become a kind of "standard candle" against which luminosity distance may be measured.

3.5 | Cosmic Distances with Standard Sirens

To typical astronomy instrumentation, each gravitational event seemed completely dark—the mass and electromagnetic fields around the merging black holes were insufficient to create any signal other than gravity. Gravitational waves, as long predicted, have provided a doorway into an otherwise inaccessible part of the cosmos. Initially, gravitational-wave astronomy did not overlap considerably with more conventional astronomy till 17 August 2017 when a gravitational-wave signal, followed by a burst of gamma rays, triggered one of the most intense observing campaigns in the history of astronomy, and with this multi-messenger astronomy was born.
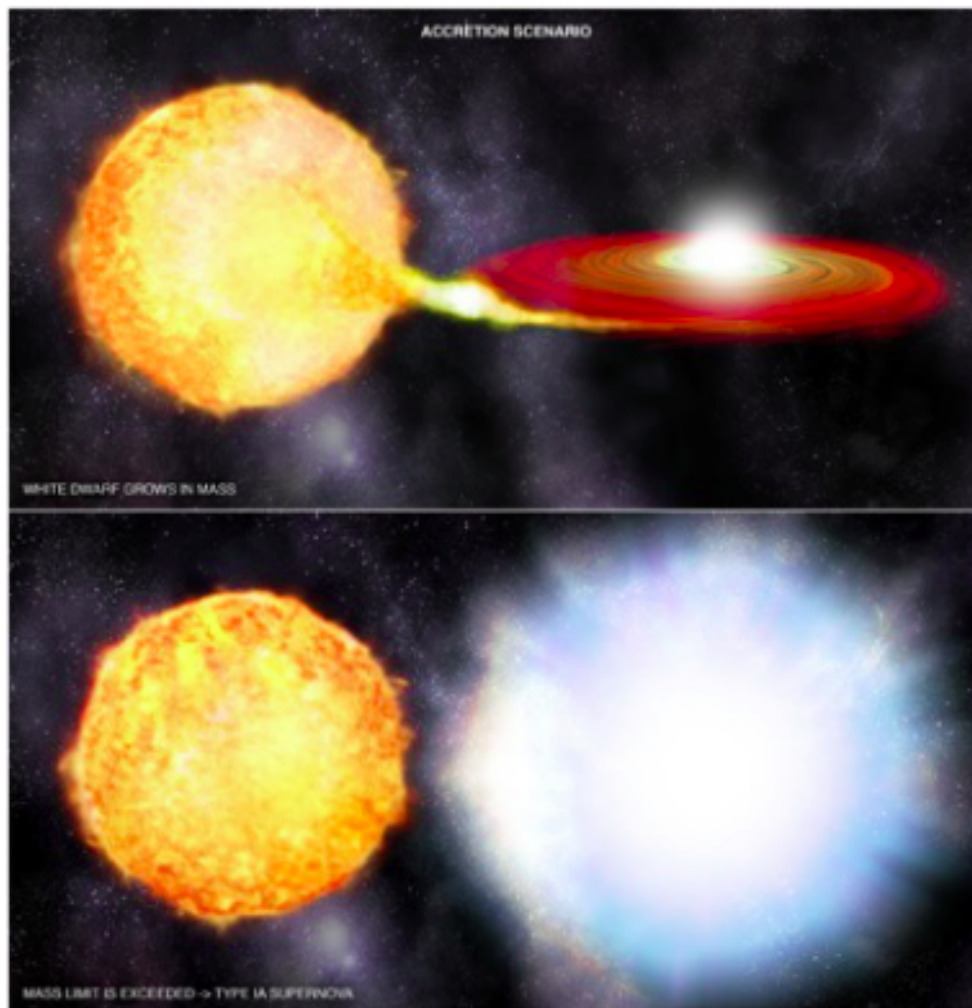
Figure 3.3: White dwarf accreting matter from a red giant companion and then exploding as a SNIa

Because gravitational waves encode the distance to their source, GW170817 gave another achievement to the astronomical community: the first determination of the local cosmic expansion rate—the Hubble constant—via gravitational waves. This watershed moment ushered forth a fundamentally new method of measuring the dynamics of the universe: the standard-siren methodology.

Standard sirens are excellent distance measurement tools. The standardized amplitude gives us the idea of how far the source is. The gravitational waves from the merger events are ripples in the spacetime fabric which due to the nature of the medium it is traversed, doesn't lose it's energy on interaction with any gravitating object, be it baryonic matter or exotic matter.

Testing the performance of Variable Chaplygin Gas Model in two different energy spectrum, the electromagnetic radiations (Standard Candles) and gravitational waves (Standard

Sirens) which are originated from two different events is a solid way to test the ability of the model to mimic the nature of the Universe.

3.5.1 | Properties of Gravitational Waves

Many properties of the metric tensor $h_{\nu\mu}$ are analogous to those of the vector potential that characterizes electromagnetic radiation. Therefore, we will be able to see many similarities between electromagnetic radiation and gravitational waves. For instance, much like electromagnetic radiation's electric and magnetic fields, gravitational waves are orthogonal to their direction of propagation. Both electromagnetic and gravitational waves have two polarizations. The electromagnetic basis polarizations point along two orthogonal axes in the plane perpendicular to the direction of propagation, and the electric force that a passing wave exerts on charges can be decomposed into components along those basis directions. Gravitational waves also exert forces normal to the propagation direction, but they act tidally, stretching along the perpendicular axis. If the wave propagates along the z-axis, one polarization stretches and squeezes along the x- and y-directions. That polarization is conventionally labelled h_+. The other polarization, h_x, stretches and squeezes along axes rotated by 45° from the x- and y-axes. For
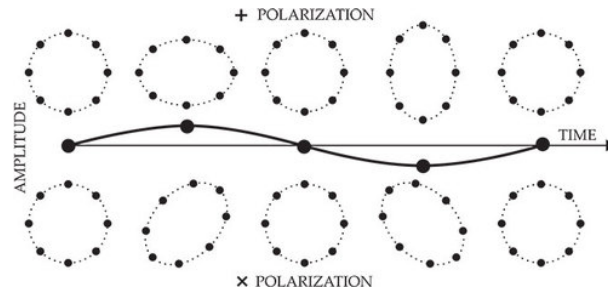

Figure 3.4: Gravitational waves polarization

sources moving at much less than the speed of light, electromagnetic radiation is described by the vector potential A that arises from a source's time-varying electric dipole moment p:

$$A_j = \frac{\mu_0}{4\pi} \frac{1}{D} \frac{dp_j}{dt} \qquad (3.4)$$

Here, D is the distance from the source, μ_0 is the permeability of free space, and the index j describes three spatial dimensions. The dipole moment is

$$\mathbf{p} = \int \rho_c \mathbf{r}' dV' \qquad (3.5)$$

where ρ_c is the charge density. There exisits analogous result for gravitational waves i.e. quadrupole formula

$$h_{jk} = \frac{2G}{c^4} \frac{1}{D} \frac{d^2 I_{jk}}{dt^2} \qquad (3.6)$$

21

where j,k are spatial and I_{jk} is the source's mass quadrupole moment

$$I_{jk} = \int_{\text{source}} \rho_{\text{m}} \left[r'_j r'_k - \frac{1}{3} \left(r' \right)^2 \delta_{jk} \right] dV' \tag{3.7}$$

where ρ_c is the source's mass density. Now, our aim is to express mass quadrupole moment in some quantities which can be easily measured and thus by using this we can measure the distance to the source without any reference to the cosmic distance ladder. Binary inspiral allows for a determination of the distance to the source.

3.5.2 | Binary inspiral: A Standard Siren

Consider a binary in a circular orbit. The gravitational waves it emits take energy from the orbit causing the binary's components to spiral toward each other. As the separation decreases lowers, the orbital frequency increases, causing higher energy loss due to gravitational waves, which causes the orbital separation to fall further, and so on. The binary therefore chirps; gravitational waves increase in frequency and amplitude as they go from low to high frequency. From Kepler's law and a well-known formula that relates the power emitted in gravitational waves to the binary's changing quadrupole moment, it is possible to show that

$$\frac{d\Omega}{dt} = \frac{96}{5} \left(\frac{GM}{c^3} \right)^{5/3} \Omega^{11/3} \tag{3.8}$$

where Ω is the frequency of the orbit, $M = (m_1 m_2)^{3/5} (m_1 + m_2)^{-1/5}$ is the chirp mass and m1 and m2 are the masses of the binary members. From the above equation, we find that the rate of change of the frequency depends only on one parameter: the chirp mass. Once we know the chirp mass, we can know how the frequency is changing at any point in the evolution of the binary system.

Let us consider a circular orbit such that the normal to its orbital plane makes an angle i to our line of sight. With that convention, i = 0° means the binary is viewed head on, and i = 90° corresponds to an edge-on view. The wave amplitudes can thus be given as

$$h_+ = \frac{2c}{D} \left(\frac{G.I}{c^3} \right)^{5/3} \Omega^{2/3} \left(1 + \cos^2 \iota \right) \cos 2\Phi(t)$$
$$h_\times = \frac{4c}{D} \left(\frac{G.L}{c^3} \right)^{5/3} \Omega^{2/3} \cos \iota \sin 2\Phi(t) \tag{3.9}$$

where $\Phi(t)$ is the accumulated orbital phase and the factor of 2 multiplying $\Phi(t)$ is due to the waves' quadrupolar nature. Chirp mass can be measured by matching the gravitational wave observationally measured with the gravitational waveform model template. If it is possible to measure more than one polarization, then the ratio of their amplitudes determines the inclination angle i. Once chirp mass and inclination angle are known, the distance to the source is determined.
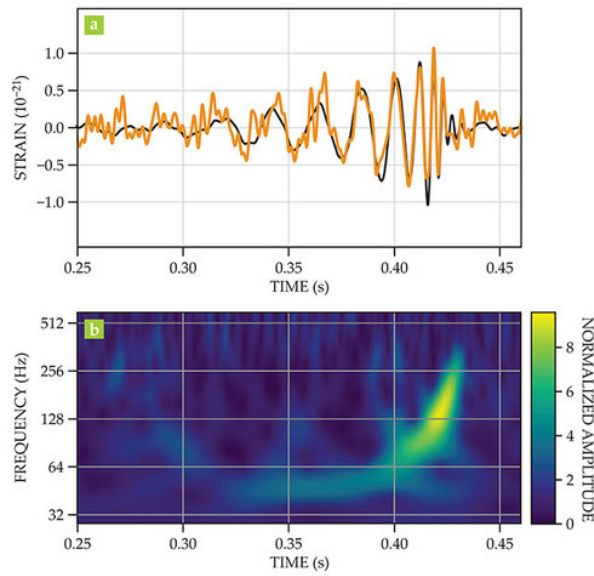
Figure 3.5: Gravitational Waveform Model Template

Binary inspiral thus acts as a standard siren as it does not require the cosmic distance ladder. To calculate the source distance, no empirical calibrations are required; the only essential assumption is that general relativity is correct.

3.6 | Bibliography Notes

Section 3.4 is influenced by the work done in Sethi et al. (2018).

23

Datasets and Calibration

4.1 | Type Ia Supernova dataset and calibration

The SCP (Supernova Cosmology Project) Union 2.1 dataset is compilation of 833 Type Ia Supernovae events collected and merged from 19 individual dataset. We have taken 580 events from the overall dataset, as these events are completely verified and could be trusted with higher level of confidence. The dataset consists of data like redshift obtained from the event, distance modulus of the event and the potential error factor involved in estimation of the distance modulus.

The luminosity distance of the Supernovae event could be expressed as a function of redshift of the event pertaining to the Variable Chaplygin Gas Model. In a flat universe in which the parameter are constrained by the Variable Chaplygin Gas Model, the luminosity distance can be expressed as

$$d_L(z, \mathbf{p}) = c(1+z) \int_0^z \frac{dz'}{H(z', \mathbf{p})} \tag{4.1}$$

where z is the redshift, H is given by

$$H^2 = \frac{8\pi G}{3} (\rho_{r0}(1+z)^4 + \rho_{b0}(1+z)^3 + \rho_{ch0}[\Omega_m(1+z)^6 + (1-\Omega_m)(1+z)^n]^{1/2}) \tag{4.2}$$

where ρ_{r0} and ρ_{b0} are the current energy densities of radiation and baryons in the universe. ρ_{ch0} is the energy density of Variable Chaplygin Gas entity consist of Dark Matter and Dark Energy. The $\mathbf{p}$ in the previous equation denotes all other parameters of the given cosmological model.

4.2 | GW Merger Events Dataset

The Gravitational Merger events are obtained from the GWOSC (Gravitational Wave Open Science Center) which has the events obtained from detectors at LIGO Hanford, LIGO Livingston and LIGO Virgo. The data set consist of many confirmed events and potentially true events which are yet to be confirmed in it. The events are collected across all the three runs: O1 (from 12 September 2015 to 19 January 2016), O2 (from 30 November 2016 to 25 August 2017) and the O3 runs, O3a (from 1 April 2019 to 30 September 2019) and O3b (from 1 November 2019 to March 2020).

There were in total 53 confirmed events in the currently data set. All these confirmed events were taken to test the efficiency of the Variable Chaplygin Gas Model to predict the luminosity distance of the event from the redshift obtained from the gravitational merger events and compare with luminosity distance obtained from the merger event by analysis of the wave received at the detector.

4.3 | Luminosity Distance from Merger Events

When a gravitational wave passes through the laser interferometer, it elongates the distance between the source and the reflector in the end in one arm and contracts the reflector length from the source in the other arm which is almost perpendicular to the elongated arm. This alternative elongation and contraction in the perpendicular arms, due to the quadrupole nature of the gravitational waves, causes path difference between the laser beams running between the arms and results in interference. The beams from perpendicular arms are made to interfere destructively in the standalone state but produce light by the interference induced by the passage of gravitational waves. The extent of elongation or contraction is determined by the amplitude of the gravitational wave passing the detector.

Since gravitational waves distort the geometrical length between the arms to cause interference, the amplitude of the laser beam from the interference pattern is directly related to the amplitude of the gravitational wave signal from the merger event. The gravitational waves weakly interact with matter, so the amplitude measured in the detector is an absolute quantity that one could measure from the merger events which provides insights about the events.

The amplitude of the wave/signal from the merger event is a function of linear separation between the binary, angular velocity of the system and also inversely proportional to the distance at which the event has occurred. This amplitude is a scale to quantify the energy emitted from the merger event as gravitational waves. Therefore we can express Luminosity of the merger event as a function of angular velocity, angular separation and distance. This luminosity is analogous to the luminosity described for stellar objects in electromagnetic counterparts.

$$h = \frac{G^{5/3}}{c^4} \frac{\mu a^2 \omega^2}{r} \tag{4.3}$$

where, h is the Amplitude of the wave , μ is the reduced mass of the system = $\frac{m_1 m_2}{m_1 + m_2}$, m_1 and m_2 are the mass which are part of the binary system, a is separation between masses, r-distance between observer and ω - orbital velocity.

$$L = \frac{dE_{GW}}{dt} \approx \frac{G}{c^5} h^2 \omega^2 \approx \frac{G}{c^5} \mu^2 a^4 \omega^6 \tag{4.4}$$

where, $\frac{dE_{GW}}{dt}$ is the rate of energy emitted by the binary event as gravitational waves.

Luminosity is a measure of energy emission from a given source. In case of binary merger events, the energy is transferred from the lost orbital energy of the binary system as the masses inspiral towards each other. So, the ratio between the frequency and the rate of change of frequency is proportional to the ratio between the separation of the mass in the system and the rate of change of this separation at successive orbits.

$$\frac{\omega}{\dot{\omega}} = \frac{-3}{2}\frac{a}{\dot{a}} = \frac{f}{\dot{f}} \tag{4.5}$$

where, f = $\frac{\omega}{\pi}$ is the frequency of the signal and $\dot{f} = \frac{\dot{\omega}}{\pi}$ is the rate of change in frequency

The ratio of frequency to the rate of change of frequency can be found from the waveform of the signal. The iconic chirp waveform of the gravitational wave from the detector helps us in obtaining the maximum amplitude, frequency and its ratio to the rate of change of frequency. From the above information, the luminosity distance (in Megaparsec (Mpc)) of a merger event can be found:

$$R = \frac{512}{h_{21}}\left(\frac{0.01}{\tau}\right)\left(\frac{100Hz}{f_{GW}}\right)^2 \tag{4.6}$$

the τ is the subtle expression for the ratio of the frequency of the gravitational wave to the rate of change in the frequency as the separation between the masses of the binary system gets reduced as they inspiral towards each other

$$\tau = \frac{f_{GW}}{\dot{f}_{GW}} \tag{4.7}$$

where, R - luminosity distance, h_{21} - amplitude caused by the inspiral of mass 1 and mass 2 of the binary system.

4.4 | Distance Modulus - Flat ΛCDM Model and VCG Model

The distance modulus is a logarithmic scaling term used to describe the distance of an energy radiating entity in astronomy. The distance modulus μ can be expressed as the difference between the apparent magnitude (m) and the absolute magnitude (M).

4.4.1 | Supernova Type Ia dataset

The distance modulus that is provided in the SNe-Ia dataset is given by the ΛCDM Model for a given redshift as

$$\mu_{obs} = a(t_0)r(1+z) \tag{4.8}$$

where a is the scale factor. The scale factor (a) in a flat universe can be expressed as $\frac{1}{(1+z)}$. t_0 is the Hubble Time which is $\frac{1}{H_0}$, where H_0 is the Hubble Parameter value in the current epoch. z is the redshift value of the entity under study.

The r in Eq. (3.8) is the coordinate distance. In a flat ΛCDM model universe, the r is expressed as

$$r = \int_t^{t_0} \frac{c\,dt}{a(t)} = \frac{c}{a_0 H_0} \int_0^z \frac{dz'}{h(z')} \tag{4.9}$$

The a_0 is the value of the scale factor in the observer's immediate surrounding. It is found to numerically equal to 1. The h is Hubble parameter value for the region of space of the given redshift. The h is expressed as

$$h(z) = \left[(1 - \Omega_{total})(1+z)^2 + \Omega_m(1+z)^3 + \Omega_\Lambda(1+z)^p \right]^{1/2} \tag{4.10}$$

in a flat universe, Ω_{total} = 1 and p is numerically equal to 1. So, the equation becomes

$$h(z) = \left[\Omega_m(1+z)^3 + \Omega_\Lambda \right]^{1/2} \tag{4.11}$$

so,

$$\mu_{obs} = \frac{1}{H_0^2(1+z)} \frac{c}{a_0} \int_0^z \frac{dz'}{\left[\Omega_m(1+z')^3 + \Omega_\Lambda \right]^{1/2}} \tag{4.12}$$

the reason why the redshift (z) inside the integral is dashed is to differentiate it with the redshift term outside the integration, and to denote that the denominator of the integral as a variable entity unlike the redshift term outside the integral.

The redshift of the given supernova event is used to calculate the distance modulus of the event and it is available in the SCP dataset.

With the Variable Chaplygin Gas Model, the distance modulus is given as

$$\mu_{th} = 5 \log d_L(z) - 5 \log h + 42.38 = 5 \log d_L(z) + 5 log \left(\frac{cH_0}{1Mpc} \right) + 25 \tag{4.13}$$

the d_L is obtained from equation 3.1

4.4.2 | Gravitational Wave Merger dataset

The standard distance modulus of the merger event is calculated from the luminosity distance obtained by the signal of the merger event as described in section 3.4 as

$$\mu_{obs} = 5 \log d_L - 5 \tag{4.14}$$

where d_L is the distance modulus obtained from the wave analysis.

The μ_{th} part is obtained from Equation 3.13, where the d_L is a function of redshift given by the wave analysis of signals from merger events. The expression for d_L is given at Equation 3.1.

The μ_{obs} is termed as observed distance modulus that is given in the database from standard cosmological model, the ΛCDM Model. The μ_{th} is the theoretical distance model, obtained from Variable Chaplygin Gas (VCG) Model.

4.5 | Bibliography Notes

This chapter is inspired from Supernova Cosmology Project and GWOSC webpages.

Gravitational Waves Data Analysis

5.1 | Gravitational Waves Data Access

5.1.1 | Packages

Some of the useful python packages used in gravitational wave astrophysics are as follows:

GWOSC - The GWOSC package helps in accessing the open data releases hosted on GWOSC from the GEO, LIGO Hanford and Livingston, and Virgo gravitational-wave observatories.

Gwpy - GWpy is a Python package providing tools for studying data from ground-based gravitational-wave detectors. GWpy provides a user-friendly, intuitive interface to the common time-domain and frequency-domain data produced by the LIGO and Virgo instruments and their analysis.

PyCBC - PyCBC is a package used to explore astrophysical sources of gravitational waves that provides functionality to analyze gravitational-wave data, detect the signatures of compact binary mergers, and estimate the parameters of a potential source.

   Note: LIGO/VIRGO data is provided in different formats:

1)HDF5: HDF5 is a high performance data software library and file format to manage, process, and store your heterogeneous data. HDF5 is built for fast I/O processing and storage. This file format is easily readable in Python, C++ and IDL. The file extension of HDF5 file is .h5.

2) Frame format (.gwf) - GWOSC data files in the gravitational wave frame file format (.gwf) may be read using the Frame Library.

3) Text file - GWOSC data is also available as a text file (.txt).

5.1.2 | Initialization

Installing and importing some packages necessary for the data analysis.

```
1   # Uncomment if running in Google Colab
2   #! pip install -q 'gwosc==0.5.4'
3   #! pip install -q 'gwpy==2.0.2'
```

Important: With Google Colab, you may need to restart the runtime after running the cell above.

```
1  import gwosc
2  import gwpy
3
4  print(gwosc.__version__)
5  print(gwpy.__version__)
```

5.1.3 │ Accessing datasets from GWOSC library

```
1  from gwosc.datasets import find_datasets, event_gps, run_segment
2  from gwosc.locate import get_event_urls
3  from gwosc import datasets
```

The GWOSC library helps to access the released public datasets from LIGO/Virgo gravitational wave runs. The gwosc.datasets.find datasets function allows to browse datasets of events, catalogs and observational runs. We can further constrain the events by the segment time, detector they were detected in, and catalog which they have been published. Below, I show how can we obtain the dataset step by step.
Request list of events from the specific detector (V1,L1,H1,G1):

```
1  H1events = find_datasets(detector="H1") # request events from other detectors
2  print(H1events)
```

It is also possible to list available catalogs (you can then choose your event from the catalog paper, for instance GWTC-2):

```
1  print("List of catalogs: \n \n", find_datasets(type="catalog"))
2
3  print("List of events: \n \n", find_datasets(type="event"))
4
5
6  gwtc = datasets.find_datasets(type='event', catalog='O3_Discovery_Papers')
7  #gwtc = datasets.find_datasets(type='event', catalog='GWTC-1-confident')
8  print('O3 events:', gwtc)
```

The run type calls the strain data sets from LIGO/Virgo observing runs. The datasets are large and have sampling frequencies from 4 - 16 [kHz]

```
1  gwrun = find_datasets(type='run')
2  print('Full datasets from runs:', gwrun)
```

We can print the GPS starting and end time of the above datasets, with the gwosc.datasets.run segment function:

```
1  #run_segment??
2
3  print(run_segment('O3a_16KHZ_R1'))
```

I will analyse the event from the 03a run (e.g. GW190521). The gwosc.datasets.eventgps function returns the GPS time since January 6, 1980.

```
1  gps_event = event_gps('GW190521-v3')
2  print(gps_event)
```

we can also recover the url associated HDF5 data files with the gwosc.locate.geteventurls function:

```
1  urls = get_event_urls('GW190521-v3')
2  print(urls)
```

5.2 | **Gravitational Waves Data Quality**

5.2.1 | Accessing data from GWpy and analysing the datasets

The data can be fetched for any particular event by function fetchopendata from the gwpy.timeseries. TimeSeries class.

```
1  #TimeSeries.fetch_open_data??
```

We can fetch the data from the event selected in the previous section (GW190521) and from a particular interferometer (e.g. Ligo Hanford H1).
For this example we choose to retrieve data for the LIGO-Hanford interferometer, using the identifier 'H1'. We can choose any of the identifier listed below:

- 'G1' - GEO600

31

- 'H1' - LIGO-Hanford

- 'L1' - LIGO-Livingston

- 'V1' - (Advanced) Virgo

In future, the Japanese observatory KAGRA will come online, with the identifier 'K1'.

5.2.2 | Handling data in the time domain

```python
from gwpy.timeseries import TimeSeries
length_seg = 128
h1_data = TimeSeries.fetch_open_data('H1', gps_event-length_seg, gps_event+length_seg, verbose=True)
print(h1_data)
```

The verbose=True flag let us see that GWpy has discovered two files that provides the data for the given interval, downloaded them, and loaded the data.

The files that are fetched are not permanently stores, so next time when you run the cell it will again download it, in some case if you don't want it to download repeatedly, one can use cache=True to store the file on your computer.

For visual representation one can plot using the plot() method of the data TimeSeries. Strain Plot using using the plot() method of the data TimeSeries.
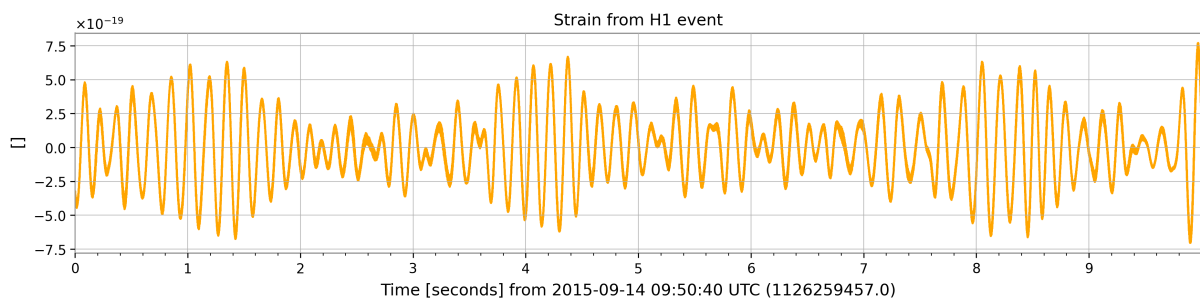
GWpy is used to deal with time series and frequency series. The gwpy.timeseries.TimeSeries.plot method allows to directly plot objects from the Timeseries class, with UTC time in the label.

```python
#type(gwpy.frequencyseries.frequencyseries.FrequencySeries)


%matplotlib inline
plot = h1_data.plot(figsize=(9, 4), title='Strain plot for event from H1');
```

5.2.3 | Handling data in the frequency domain using the Fourier transform

We can recover the frequency content of the above time series by using the gwpy.timeseries. Timeseries.fft function (based on numpy.fft.rfft) which yields a FrequencySeries instance, appropriately normalized.

```python
#TimeSeries.fft??

fft = TimeSeries.fft(h1_data)
print(fft)
```

The result is a TimeSeries, with complex amplitude, representing the amplitude and phase of each frequency in our data. We can use abs() to extract the amplitude and plot that:

```python
plot = fft.abs().plot(xscale="log", yscale="log",figsize=(6,6), title='ASD%
                      with no window')
#plt = plot
#plt.savefig('ASDH1.png',dpi=300)
```

The problem with the plot is that the FFT works under the assumption that our data are periodic, this implies that the end of our data appears to be discontinuities when transformed. To optimize this a window function is applied to the time-domain data before transforming, which can be done using scipy.signal module:

```python
from scipy.signal import get_window
window = get_window('hann', h1_data.size)
hwindow = h1_data * window
fftamp = hwindow.fft().abs()
plot_new = fftamp.plot(xscale="log", yscale="log", figsize=(6,6), title='ASD with%
                       Hann window')
```

Also instead of applying a single FFT, it is good practice to recover the spectral properties of the GW strain applying an averaging method. This can be achieved with the gwpy.timeseries. TimeSeries.asd, which returns an averaged ASD computed with the segment, into a FrequencySeries.

```python
#gwpy.timeseries.TimeSeries.asd??

asd_h1 = h1_data.asd(fftlength=2, window='hann', method="welch")
plot = asd_h1.plot(title='Welch avg. ASD from 10 to 1500 Hz', figsize=(6,6),%
```

33

```
5                    label = 'LIGO:Hanford',color='gwpy:ligo-hanford')
6    ax = plot.gca()
7    ax.set_ylabel(r'Strain noise [$1/\sqrt{\mathrm{Hz}}$]')
8    ax.set_xlim(10, 1500)
9    ax.set_ylim(1e-24, 1e-20);
```

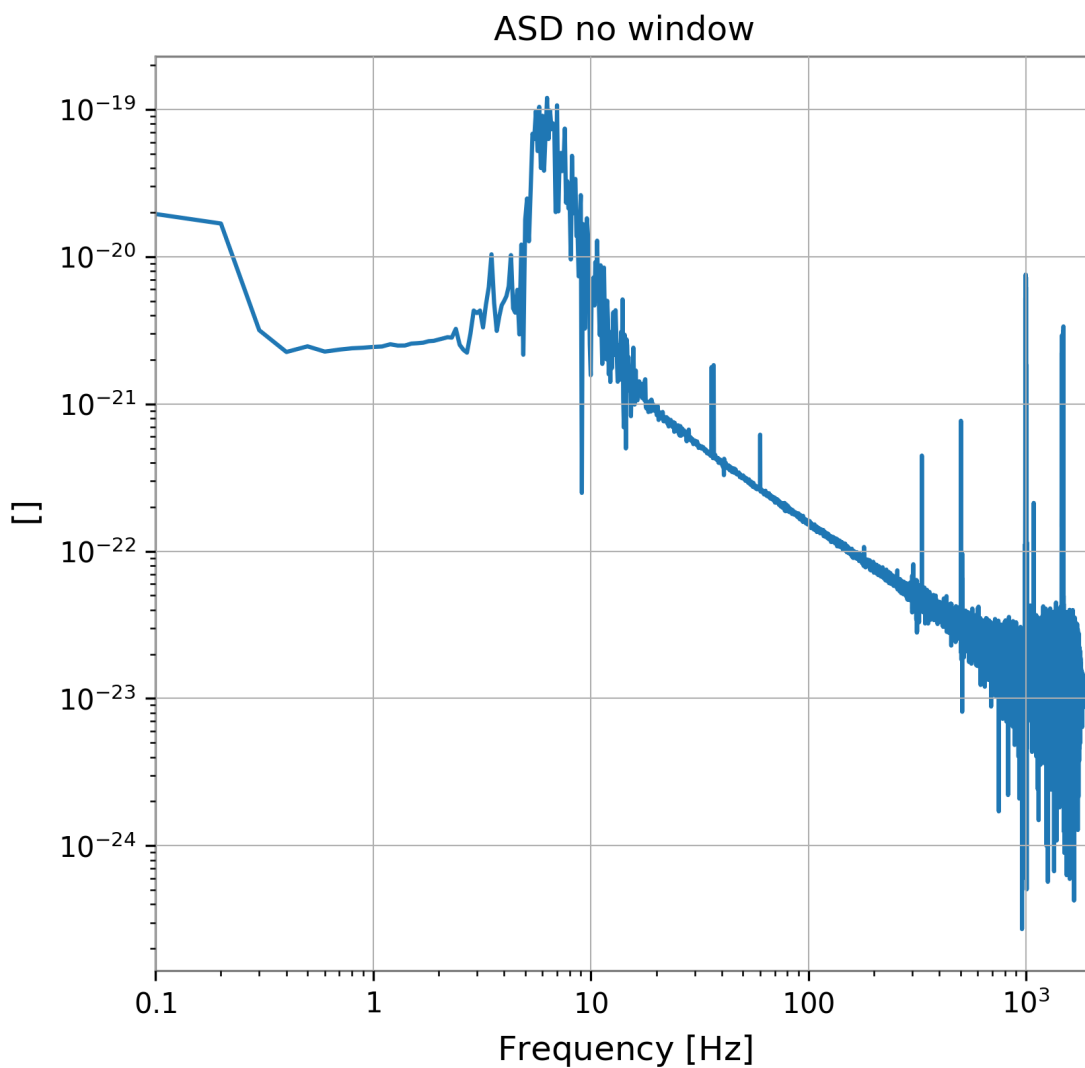Similarly the plot of Welch avg. ASD can be obtained for the other two detectors as well.
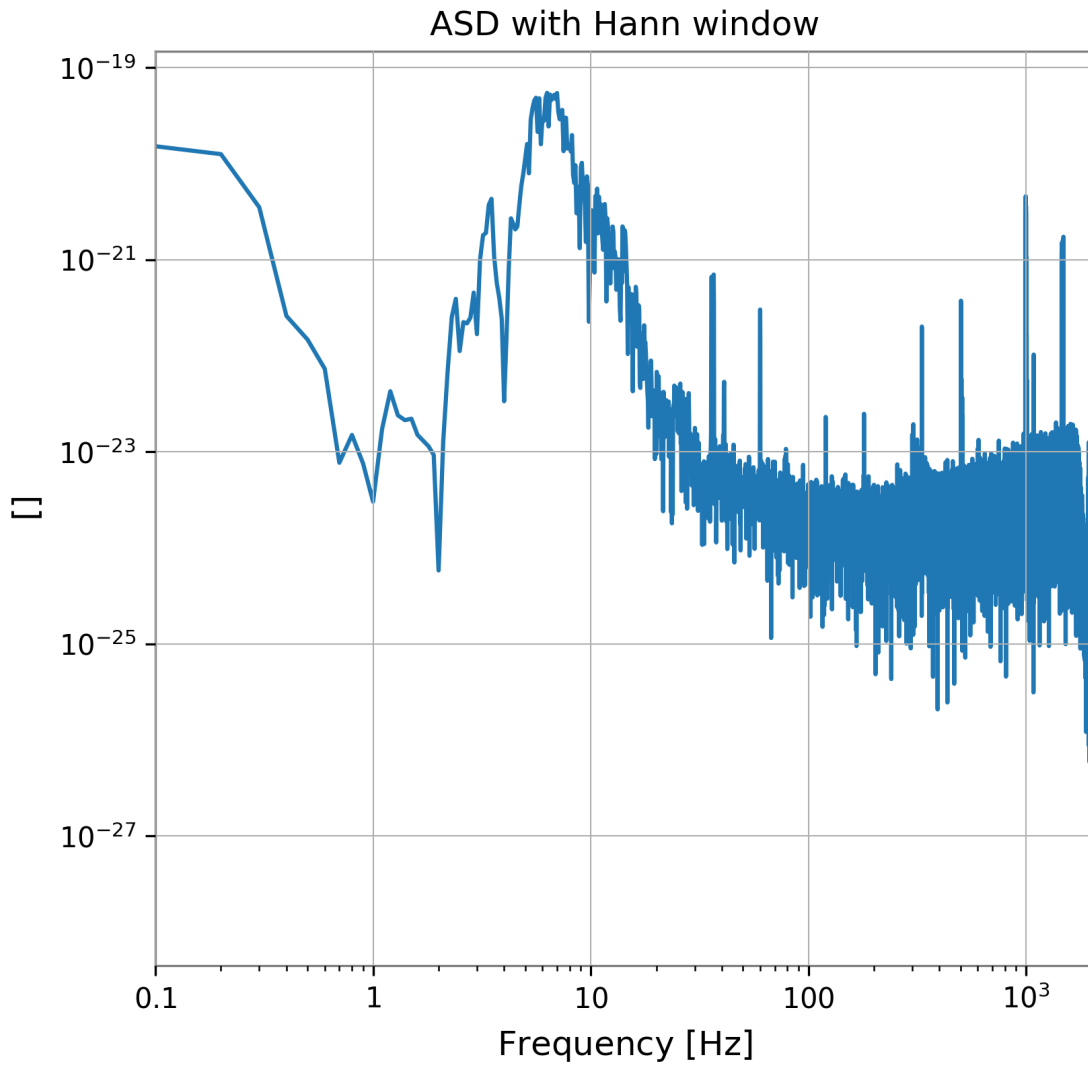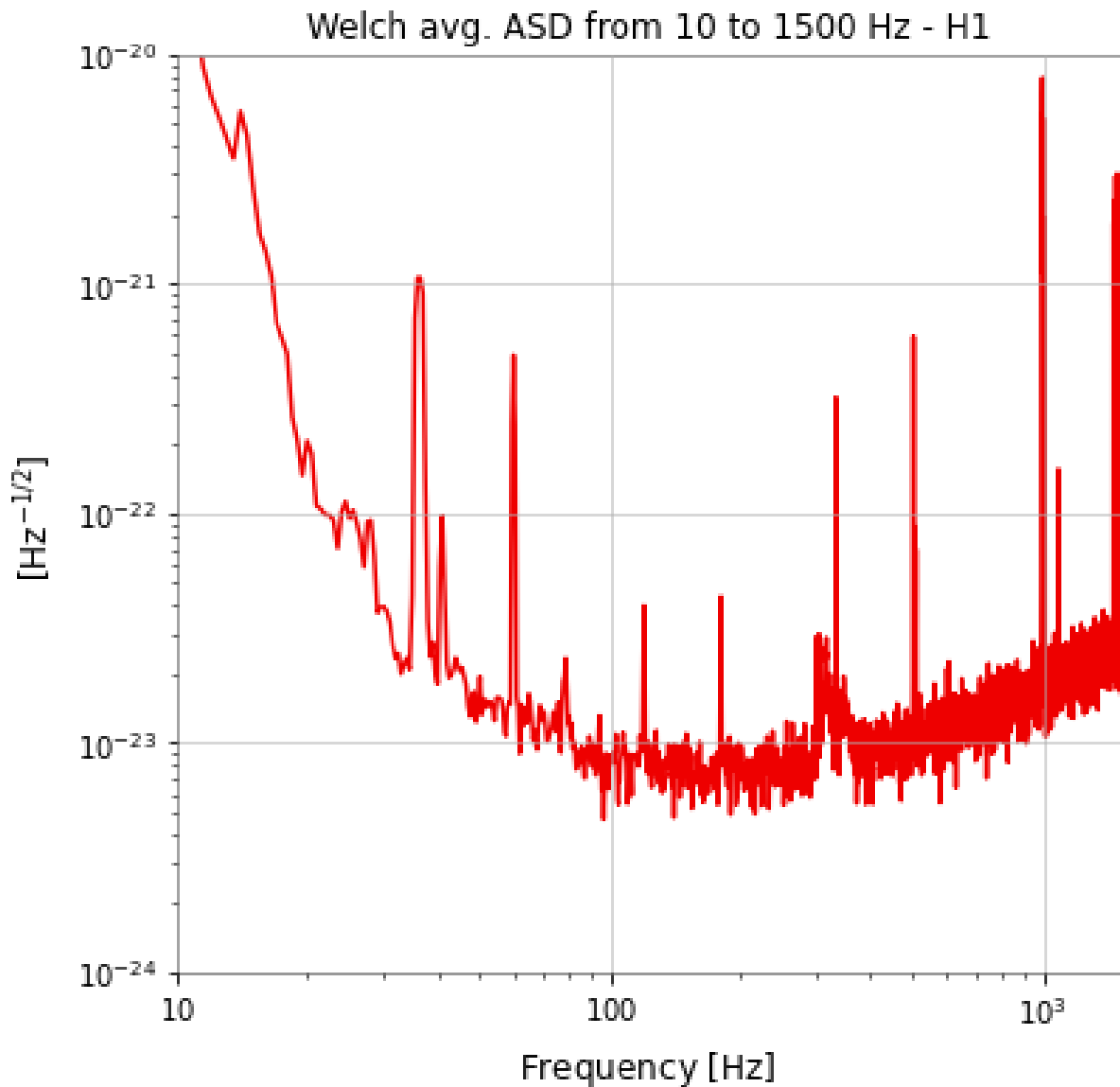

Figure 5.1: no window

Figure 5.2: 'Hann' window

This is what a typical GW detector ASD curve looks like. It is the sum of contributions by a wide variety of noise sources (seismic and newtonian, thermal, quantum etc etc). We can observe in particular some spectral lines and peaks (see for instance, the description for O2 lines `https://www.gw-openscience.org/o2speclines/`)

5.2.4 | Time-Frequency representation

The Amplitude Spectral Density(ASD) and timeseries plot is useful but only by looking at them does not specify the low Signal-to-Noise(SNR) events. Therefore, a time-frequency representation is preferred, which tracks the evolution of the ASD or PSD in time. It can be plotted using the TimeSeries methods spectrogram and/or spectrogram2.

5.2.5 | Q-transforms in GWpy

A better way is to use multi-resolution methods, such as the wavelet transform or the Q-transform, which involves logarithmic tiling in the time–frequency plane. The quantity Q is
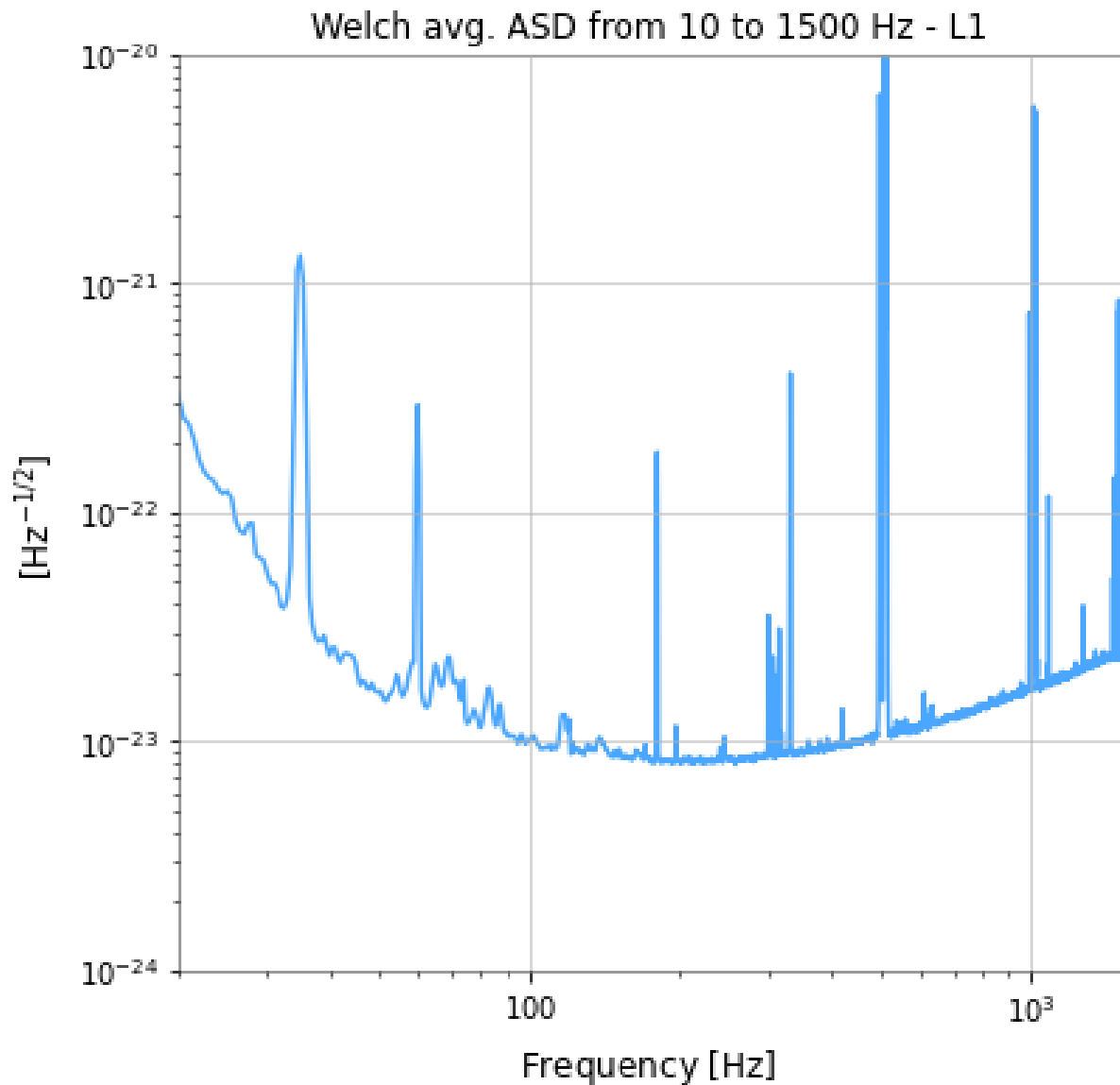
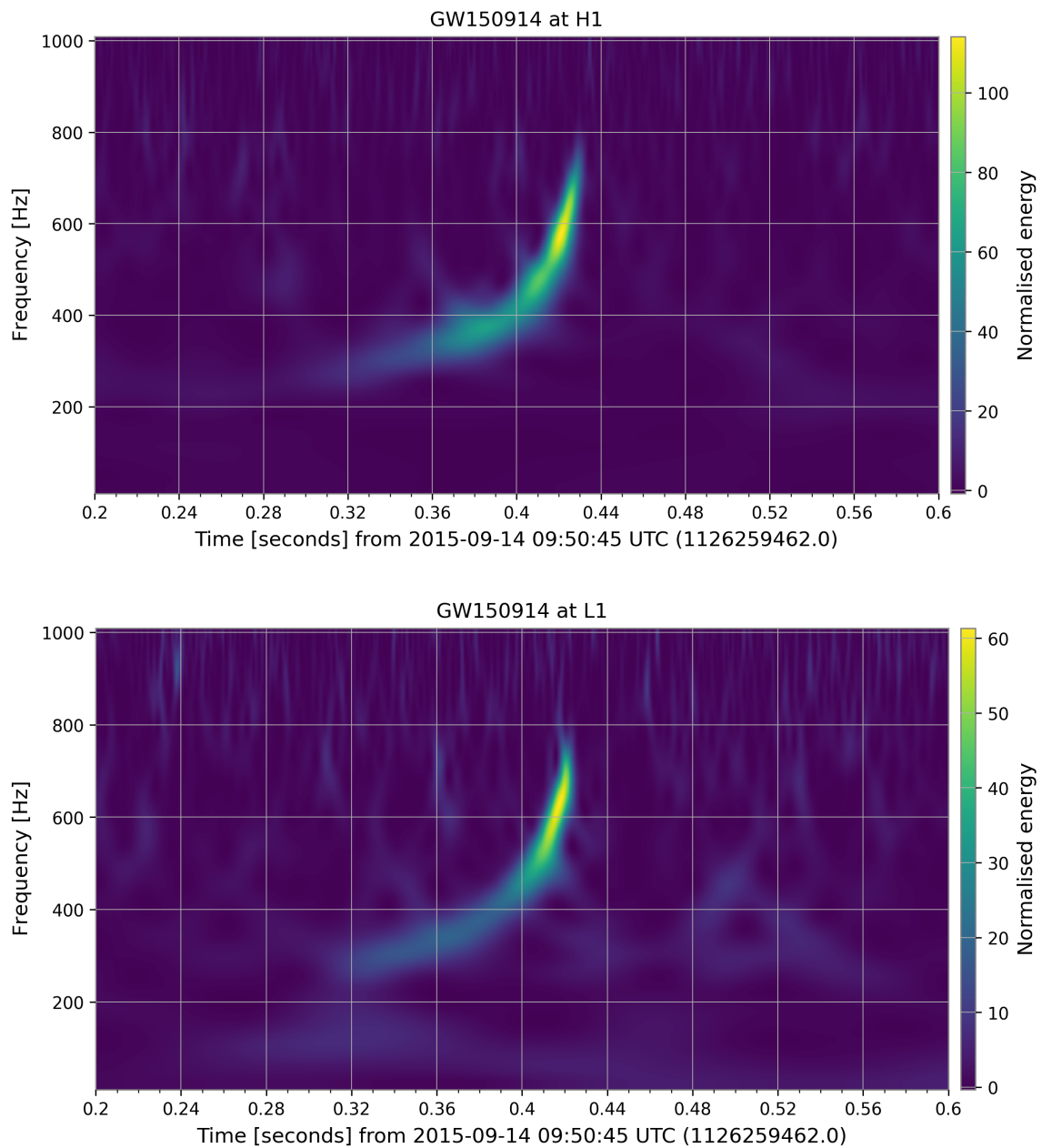a measure of the burst's aspect ratio in the time-frequency plane.

$$\boxed{\dfrac{f_c}{\sigma_f}}$$

```
1   h1_q = h1_data.q_transform(frange=(30, 200), outseg=(gps_event-0.25,gps_event+0.25))
2   # outseg to zoom around merger
3   plot = h1_q.plot(title='GW190521 at H1', figsize=(9,5))
4   plot.colorbar(label="Normalised energy");
```

Similarly the chirp can be obtained for other detectors as well.

GW150914 at H1

GW150914 at L1

5.3 | Gravitational Wave Results

5.3.1 | Generating Waveforms

Here we'll generate the gravitational waveform using one of the available waveform approximants. The waveform can be generated as a time series using get_td_waveform(). There are some additional examples using this interface here. The key parameters are the masses of the binary (given in solar masses), the time between samples (in seconds), the starting

gravitational-wave frequency (Hz) and the name of the approximant we'd like to use. A variety of approximants are available that include different physical effects.

In this example, we've chosen to use the 'SEOBNRv4_opt' approximant. This is an implementation of the model introduced in this paper. It models the gravitational waveform of inspiralling and merging black holes, and includes the ability for each black hole to spin in the same direction as the orbit (aligned spin).

There are many other models available, with different methodologies employed and physical effects modelled. A full review of the models is outside of the scope of this tutorial.
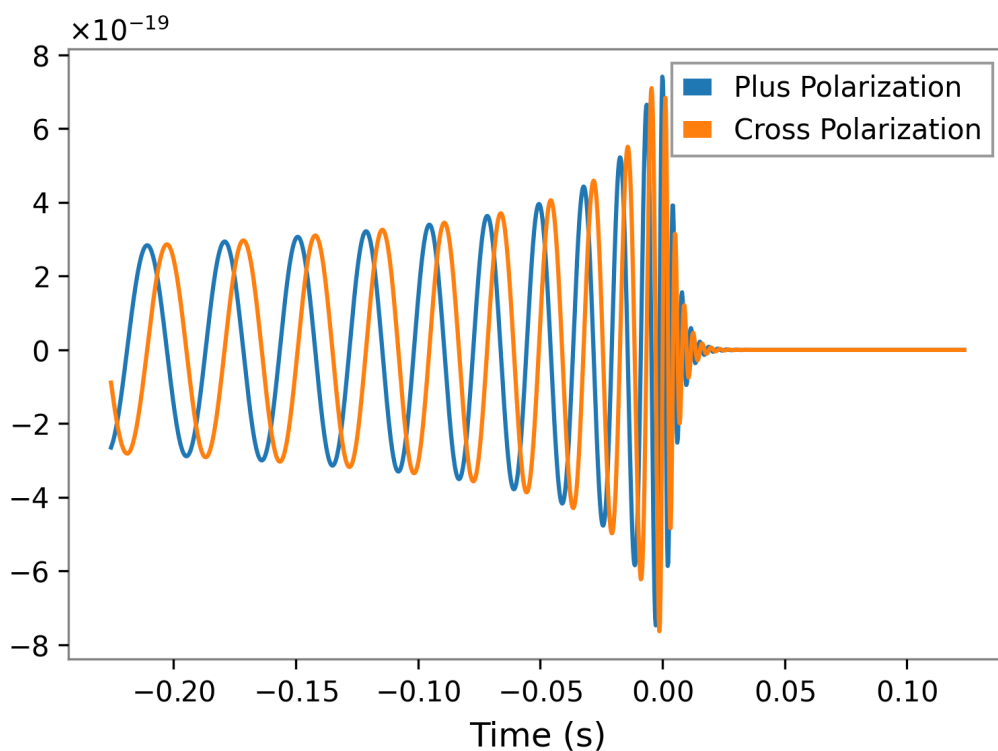
We can see that in this case, the two polarizations differ only by the phase of the signal. This is a known property of the signal, when the orbital plane of the binary does not precess (i.e. the individual black holes spins are aligned with the orbital angular momentum). In the zoom-in plot, we can see the merger itself and the ringdown that follows.

5.3.2 | Change in Binary mass affects the waveform

Below you can see how the length of the waveform increases for lower-mass binary mergers.
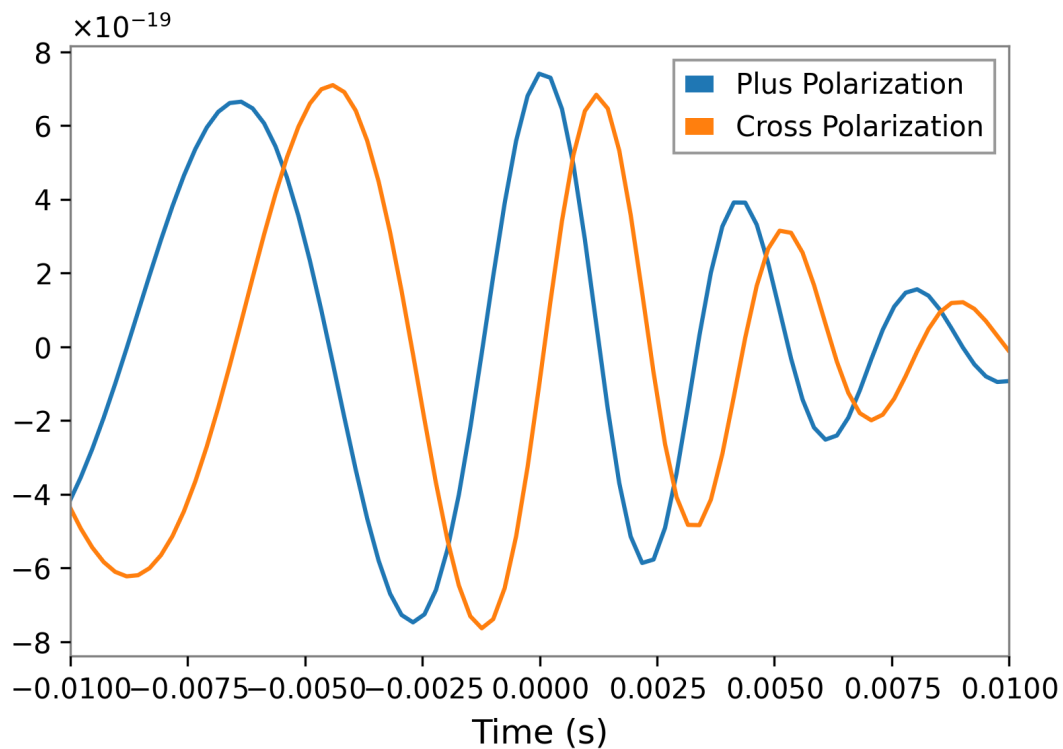
### 5.3.3 | Changing the distance of the waveform

### 5.3.4 | Matched Filtering

We will be using the PyCBC library, which is used to study gravitational-wave data, find astrophysical sources due to compact binary mergers, and study their parameters. The techniques to find astrophysical signals may not be exact but we have been consistently comparing our results with the published results along with the workshops conducted by LIGO.

5.3.4.1 | Looking for a peculiar signal in the data

If you know what signal you are looking for in the data, then matched filtering is known to be the optimal method in Gaussian noise to extract the signal. Even when the parameters of the signal are unknown, one can test for any set of parameters one is interested in finding.

5.3.4.2 | Preconditioning the Data

The purpose of preconditioning data is to reduce the dynamic range of the data and to supress low frequency behavior that can introduce numerical artefacts. We may also wish to reduce the
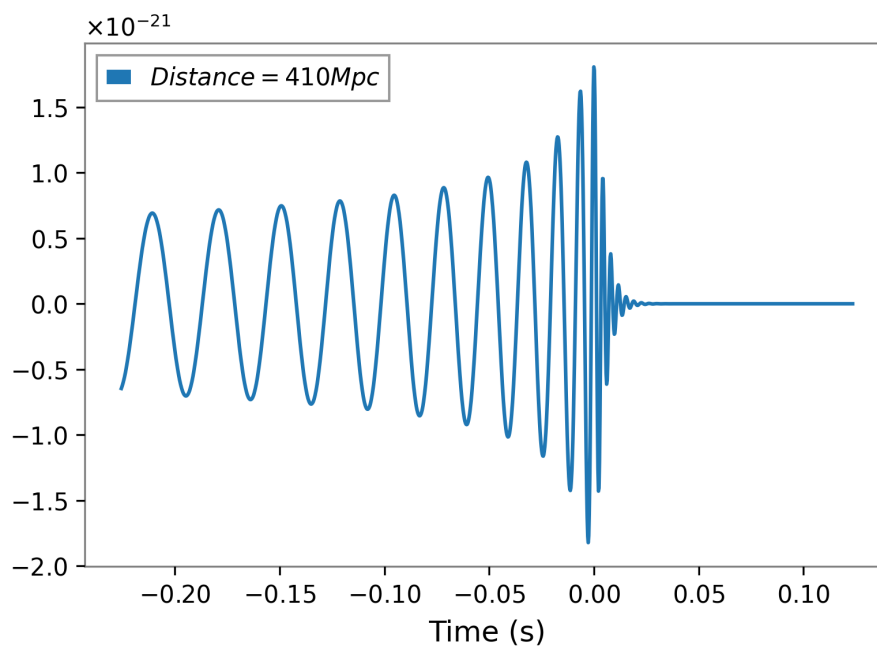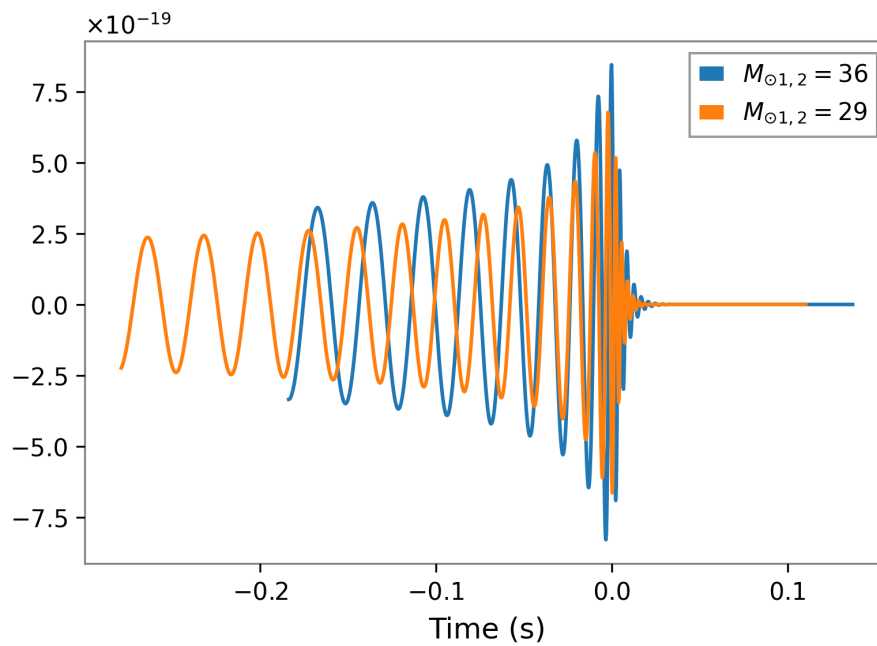
sample rate of the data if high frequency content is not important.

PyCBC contains an interface to the GWOSC catalog, so you can easily access the data and parameters of the published gravitational-wave signals.
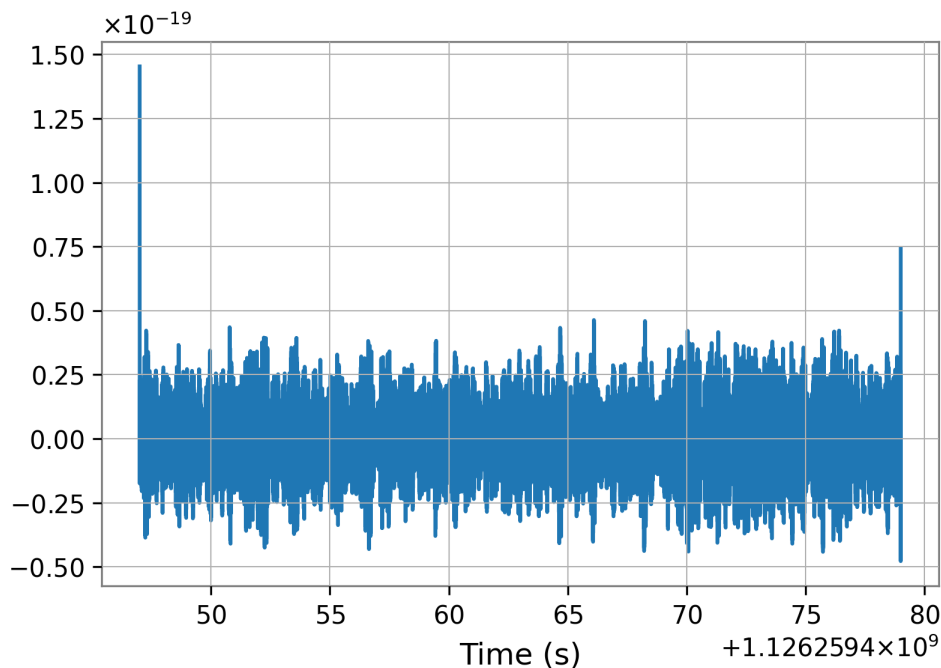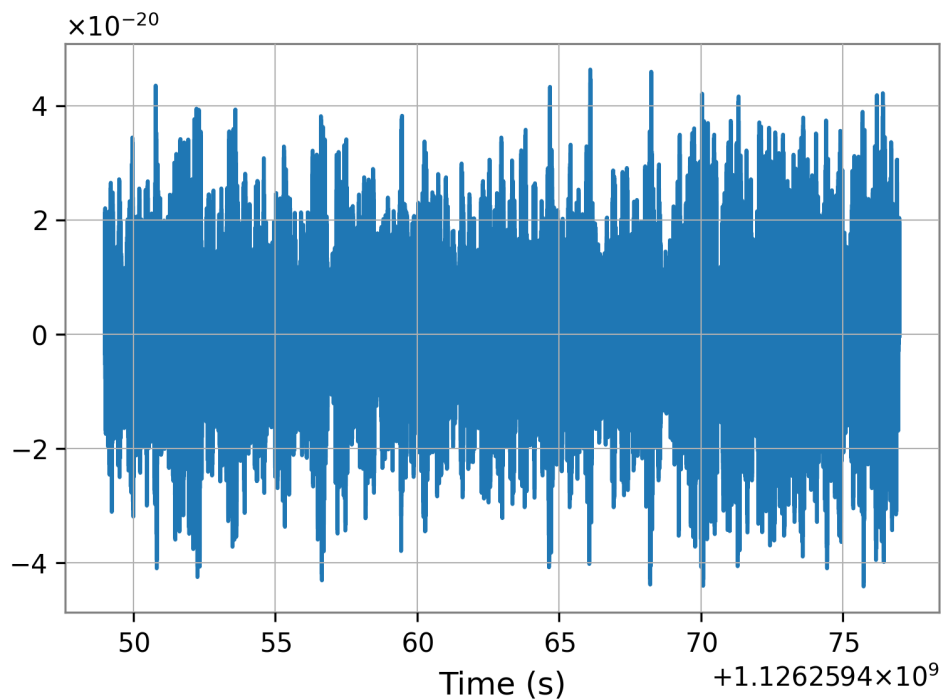
5.3.4.3 | Wrapping a filter around

Note the spike in the data at the boundaries. This is caused by the highpass and resampling stages filtering the data. When the filter is applied to the boundaries, it wraps around to the beginning of the data. Since the data itself has a discontinuity (i.e. it is not cyclic) the filter itself will ring off for a time up to the length of the filter.

Even if a visible transient is not seen, we want to avoid filters that act on times which are not causally connected. To avoid this, we trim the ends of the data sufficiently to ensure that they do not wrap around the input. We will enforce this requirement in all steps of our filtering.

5.3.4.4 | Calculating Power Spectral Density

Optimal matched filtering requires weighting the frequency components of the potential signal and data by the noise amplitude. We can view this as filtering the data with the time series equivalent of 1 / PSD. To ensure that we can control the effective length of the filter, we window the time domain equivalent of the PSD to a specific length. This has the effect of losing some information about line behavior in the detector. However, since our signals span a large frequency range, and lines are narrow, this is a negligible effect.

Important note: Computing a PSD from data that might contain signals, non-Gaussianities and non-stationarities is not trivial. In this example we use Welch's method to obtain a PSD esti-

mate. PyCBC's PSD module contains tools for measuring PSDs, or directly using pre-generated PSDs.

5.3.4.5 | Creating Your own Signal Model

Conceptually, matched filtering involves laying the potential signal over your data and integrating (after weighting frequencies correctly). If there is a signal in the data that aligns with your "template", you will get a large value when integrated over.

In this case we "know" what the signal parameters are. In a real search we would grid over the parameters and calculate the SNR time series for each one.

We will assume equal masses, and non-rotating black holes which is within the posterior probability of GW150914.

The waveform begins at the start of the vector, so if we want the SNR time series to correspond to the approximate merger location, we need to shift the data so that the merger is approximately at the first bin of the data.

The cyclic_time shift method shifts the timeseries by a given amount of time. It treats the data as if it were on a ring so points shifted off the end of the series reappear at the start.

Note that time stamps are not in general affected (as the start time of the full array is shifted), but the index of each point in the vector is.

By convention, waveforms returned from gettdwaveform have their merger stamped with time zero, so we can use the start time to shift the merger into position.
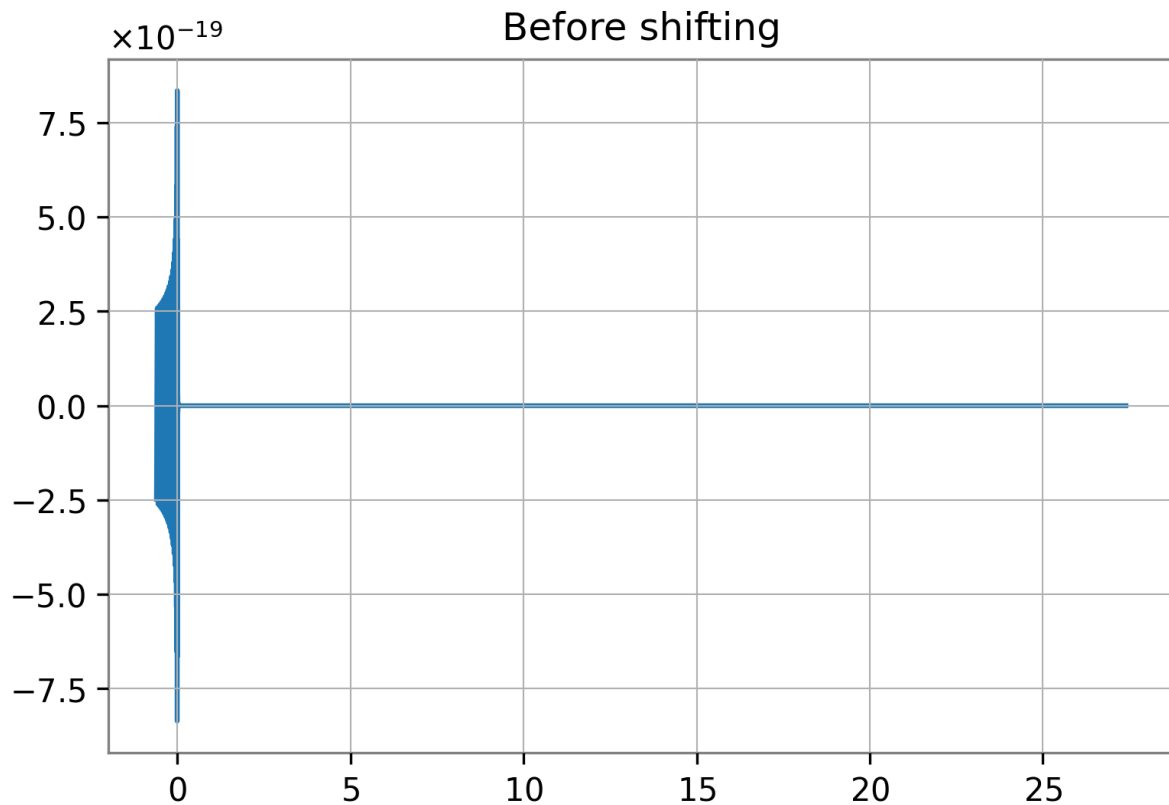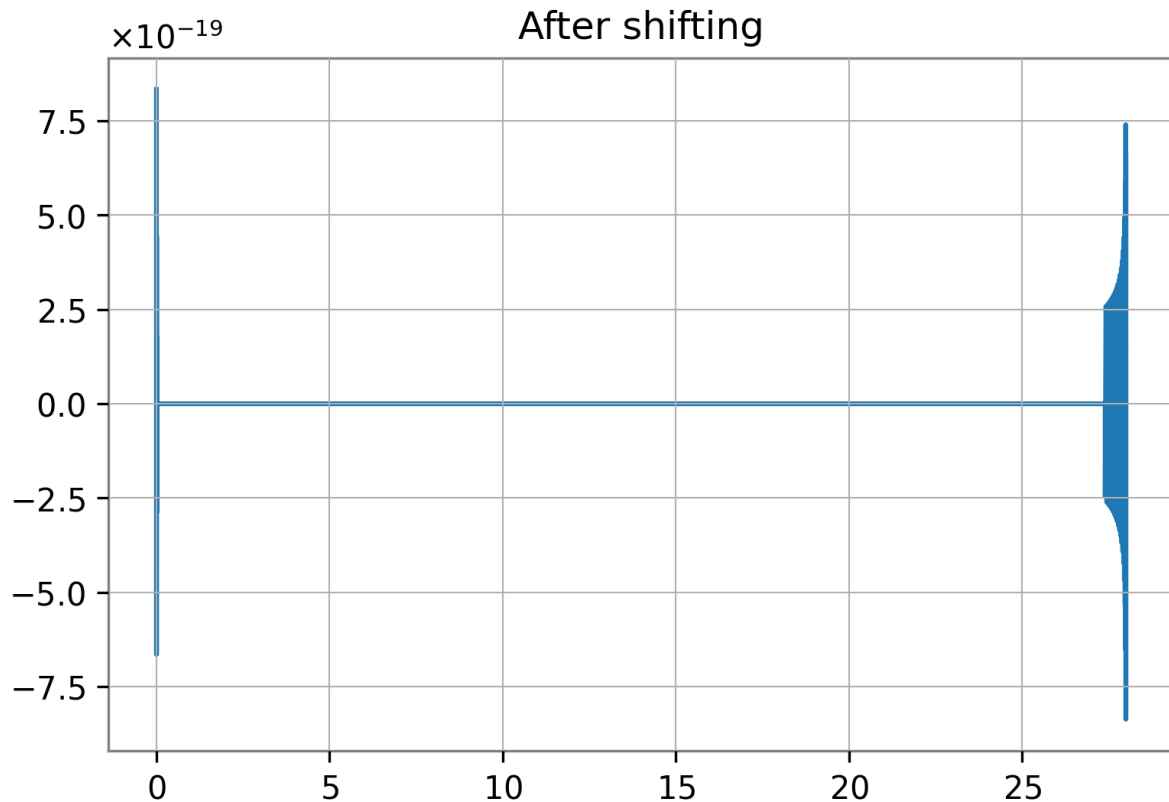
5.3.4.6 | Calculating the Signal-to-Noise Time Series

In this section we will calculate the signal-to-noise time series for our template. We'll take care to handle issues of filter corruption / wraparound by truncating the output time series. We need to account for both the length of the template and 1 / PSD.

We found a signal at 1126259462.4248047s with SNR 19.677089013145903

5.3.4.7 | Aligning and Subtracting the Proposed Signal

In the previous section we found a peak in the signal-to-noise for a proposed binary black hole merger. We can use this SNR peak to align our proposal to the data, and to also subtract our proposal from the data.

5.3.4.8 | Overlapping the signal and the data

To compare the data an signal on equal footing, and to concentrate on the frequency range that is important. We will whiten both the template and the data, and then bandpass both the data and template between 30-300 Hz. In this way, any signal that is in the data is transformed in the same way that the template is.
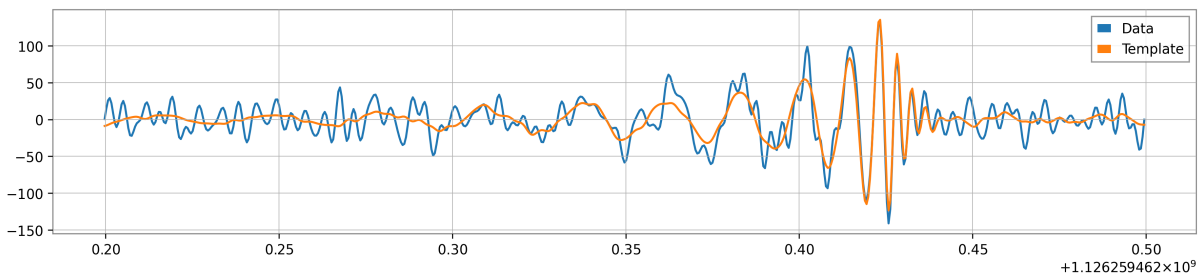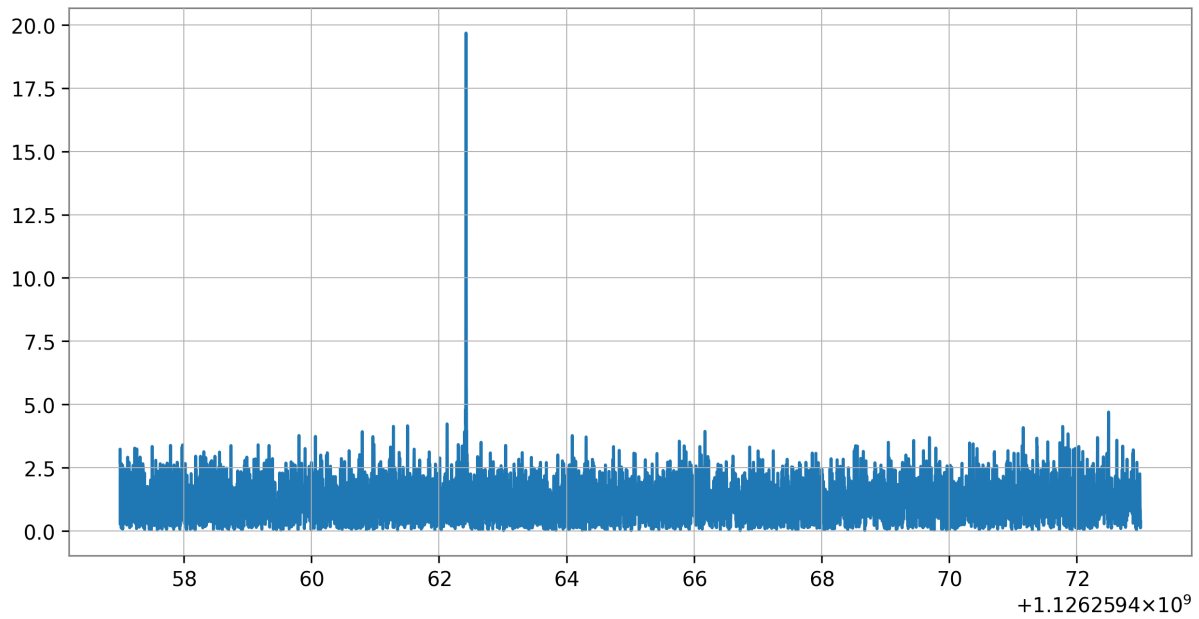
5.3.4.9 | Subtracting the Signal from the Data

Now that we've aligned the template we can simply subtract it. Let's see below how that looks in the time-frequency plots!

Signal Subtracted from H1 Data

<div align="right">

6

</div>
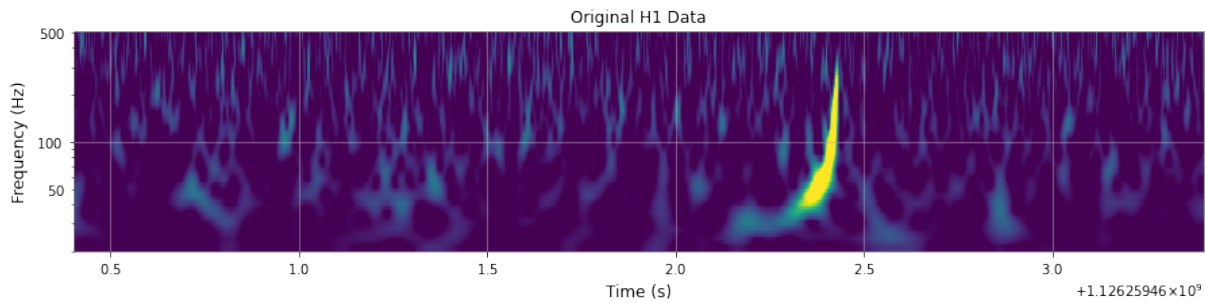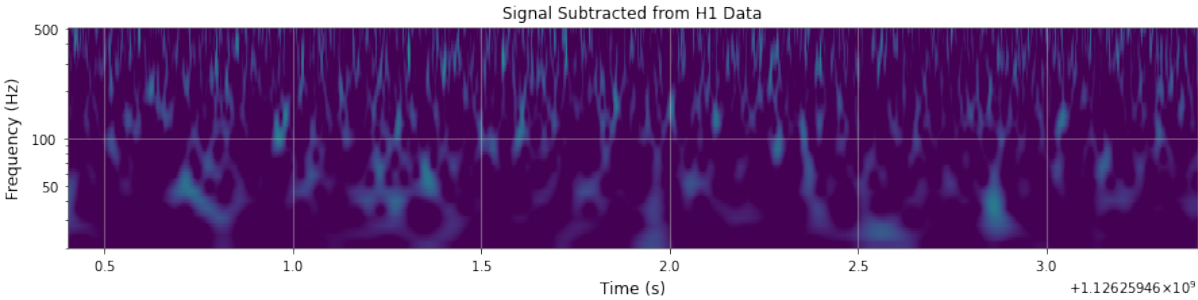
Statistical Analysis

6.1 | Overview

In order to find the right combination of the constrains Ω_m and n for which the model provides best fit of the luminosity distance and the distance modulus, a χ^2 test is conducted between the observed values in the dataset and the calculated values from the model. χ-squared is a test to verify a hypothesis proposed to explain the distribution in a given dataset. The hypothesis or the equation that is devised to fit the distribution of the data-points from given parameters are generally termed as Null Hypothesis. These null hypothesis when tested with a χ^2 test provides a numerical value which defines the goodness of the hypothesis. This numerical value should be equal to or be around the numerical value of the total number of data-points involved in the dataset. χ-squared test provides a clear picture on the performance of the model.

6.2 | Hypothesis Testing

A statistical hypothesis test is a statistical inference procedure that is used to determine a conclusion from two conflicting hypotheses, i.e. null hypothesis and alternative hypothesis. If the result from the sample has the probability of occurence greater than significance value, assuming null hypothesis is correct, then null hypothesis and sample result are not statistically significant and vice versa. In other words, the sample thus leads to acceptance of our null hypothesis.

6.3 | Chi Square Distribution

The chi-squared distribution with k degrees of freedom is the distribution of a sum of the squares of k independent standard normal random variables, which is used in inferential statistics, notably in hypothesis testing and in construction of confidence intervals. The chi-squared distribution is used primarily in hypothesis testing. The chi-squared distribution has one parameter: a positive integer k that specifies the number of degrees of freedom. The chi-squared

distribution is applied in modeling of natural phenomena and used in Pearson's chi-squared test.

6.4 | Pearson's χ^2 Test

To see if there is a discrepancy between the theoretical population parameter and the observed data, a Chi-square test is used. Karl Pearson developed this test for categorical data analysis and distribution in 1900. As a result, it was referred to as Pearson's chi-squared test. The chi-square test is used to quantify the likelihood of observations made under the premise that the null hypothesis is true. A hypothesis is a possibility that a certain condition or statement is true, which we may then test.

The standard equation to determine the goodness value of the χ^2 test for distance modulus is given by

$$\chi^2 = \sum_i \left[\frac{\mu_{th}^i - \mu_{obs}^i}{\sigma_i} \right] \tag{6.1}$$

where μ_{th} is the distance modulus value obtained from the theoretical calculation of the cosmological model and μ_{obs} is the observed value of distance modulus in the dataset. σ is the possible magnitude of error in the observed distance modulus given by the dataset. The $\left[\frac{\mu_{th} - \mu_{obs}}{\sigma} \right]$ is calculated for each data-point and is summed for the total dataset.

In order to make to attribute the performance of other non constrained factors like the Hubble Parameter H_0, the equation is modified as

$$\chi^2 = \sum_i \left[\frac{\mu_{th}^i - \mu_{obs}^i}{\sigma_i} \right] - \frac{C_1}{C_2} \left(C_1 + \frac{2}{5} \ln 10 \right) - 2\ln h \tag{6.2}$$

The terms C_1 and C_2 are given by

$$C_1 = \sum_i \frac{\mu_{th}^i - \mu_{obs}^i}{\sigma_i^2} \tag{6.3}$$

$$C_2 = \sum_i \frac{1}{\sigma_i^2} \tag{6.4}$$

h is the dimensionless Hubble parameter

$$h = \frac{H_0}{100(km)(s^{-1})(Mpc^{-1})} \tag{6.5}$$

6.5 | Bibliography Notes

The Equations are derived from primary work done in Sethi et al. (2018)

The technical aspects of the χ-squared test and χ^2 goodness value in Section 4.1 is inspired from Chi (2010)

Discussion & Conclusions

7.1 | Discussion

7.1.1 | Calibration with SNe-Ia Dataset

Before analyzing the performance of Variable Chaplygin Gas Model with Gravitational Merger Event, it has to be calibrated with respect to the SCP Union Type Ia supernovae data to compare the results of the model generated to the previous published results on the model to provide credibility to the model performance on Merger events. Variable Chaplygin Model has a provided a best fit to the SNe-Ia dataset for $\Omega_m = 0.15$ and n = 0.79 with a χ^2 goodness value of 566.296 for the distance modulus.
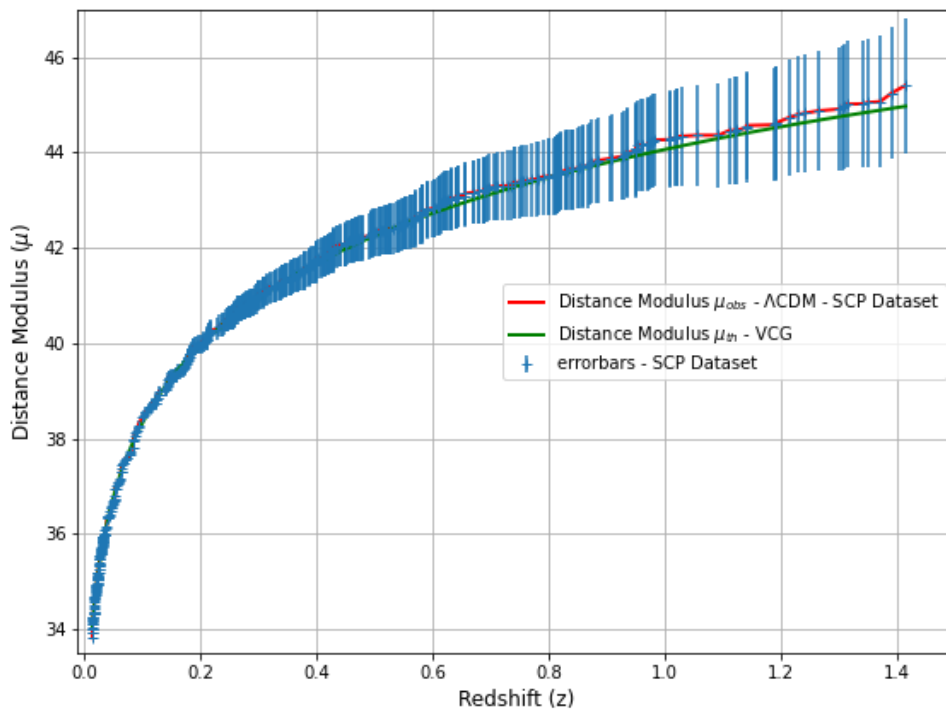

Figure 7.1: Performance of VCG Model to determine Distance Modulus (Green) with respect to the Distance Modulus from SCP Dataset (Red) against Redshift - Ω_m=0.15, n = 0.79 and H_0=69.8

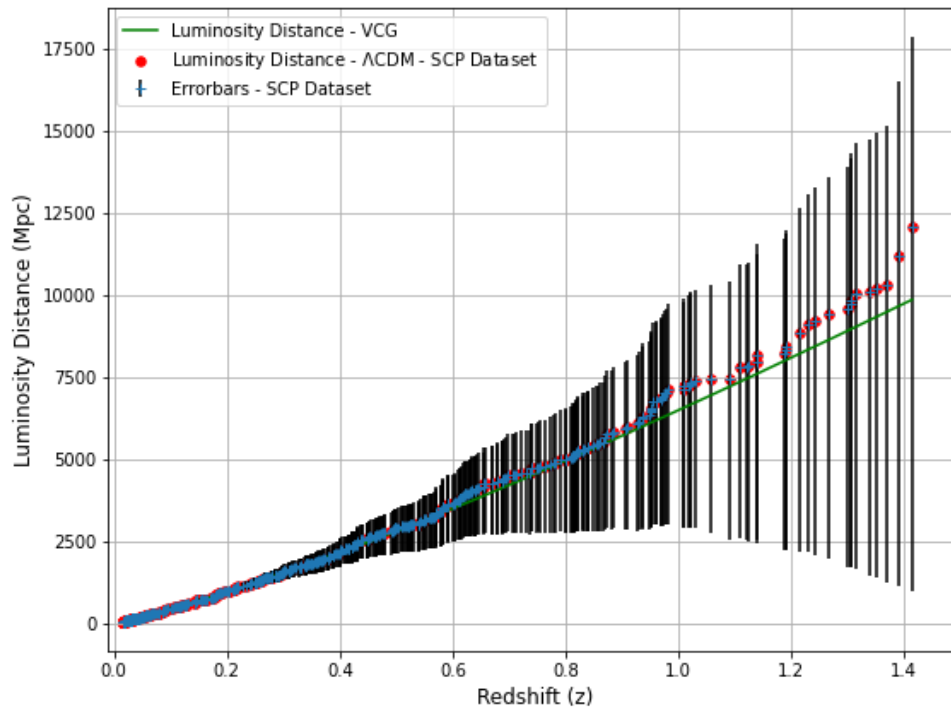The performance VCG Model to determine luminosity distance is also included

Figure 7.2: Performance of VCG Model to determine Luminosity Distance (Green) with respect to the Luminosity Distance from ΛCDM Model (Red) against Redshift - Ω_m=0.15, n = 0.79 and H_0=69.8

The graph depict the performance of the VCG devised against standard SCP Dataset. This provides credibility to the model has the predicted values of Ω_m and n closer to values from published papers: Guo Zhong [Ω_m=0.25, n=-2.9] and Sethi [Ω_m=0.22, n=-2.8].

7.1.2 | Model performance on Gravitational Merger Events

The Variable Chaplygin Gas Model, provided a best fit to the gravitational wave merger events obtained from GWOSC, for Ω_m = 0.17 and n = -8.7 with a χ^2 goodness value of 0.388 for the distance modulus.

Similarily the perforance of VCG Model in determining Luminosity distance is given in the following plot
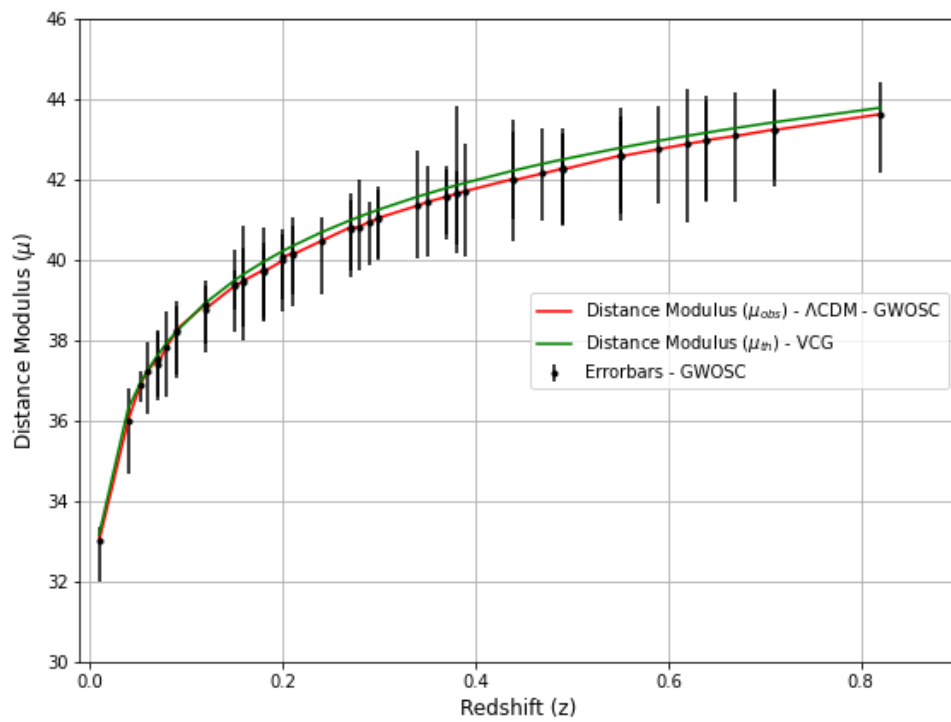
Figure 7.3: Performance of VCG Model to determine Distance Modulus (Green) with respect to the Distance Modulus from ΛCDM Model (Red) against Redshift from GWOSC Dataset - Ω_m=0.17, n = -8.7 and H_0=69.8

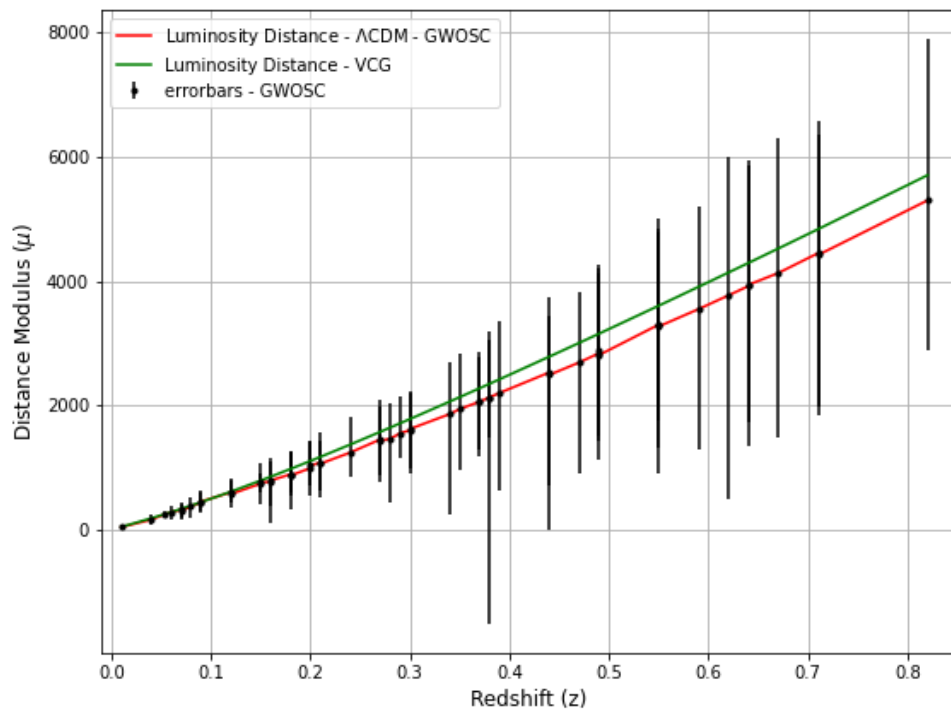Figure 7.4: Performance of VCG Model to determine Luminosity Distance (Green) with respect to the Luminosity Distance from ΛCDM Model (Red) against Redshift from GWOSC Dataset - Ω_m=0.17, n = -8.7 and H_0=69.8

Future Work

8.1 | New Datasets

The GWOSC Dataset has added new confirmed events added from O3a and O3b runs. Including them into the dataset would be beneficial to constrain the cosmological parameters Ω_m and n with tighter bounds.

8.2 | Range of Constraints - Contour Plots

A contour plot to determine the validity of χ^2 goodness value will be plotted. This provides more credible proof about the modified χ^2 test that has been implemented for VCG Model.

8.3 | Determination of H_0

With the parameters obtained from χ^2 test on GWOSC dataset, we could find the value of Hubble Parameter in the current epoch within our immediate surroundings of the Universe.

8.4 | Statistical tests

We are aiming to use Markov chain Monte Carlo (MCMC) method to analyze non-gaussian uncertainties in GW merger events datasets.

References

Gw@home with ligo-india - youtube. URL `https://www.youtube.com/playlist?list=PLlQd-wufT12_kVe1QoviWj7P71wC5plb8`.

Grb 190425 | christopher berry. URL `https://cplberry.com/tag/grb-190425/`.

Cosmomc readme. URL `https://cosmologist.info/cosmomc/readme.html`.

Supernova cosmology project. URL `https://supernova.lbl.gov/union/`.

Least-squares and chi-square for the budding aficionado: Art and practice. 2010.

J. Aasi and B. P. Abbott et al. Advanced ligo. *Classical and Quantum Gravity*, 32, 2015. ISSN 13616382. doi: 10.1088/0264-9381/32/7/074001.

Rana X. Adhikari. Gravitational radiation detection with laser interferometry. *Reviews of Modern Physics*, 86, 2014. ISSN 15390756. doi: 10.1103/RevModPhys.86.121.

Bhuvan Agrawal, Geetanjali Sethi, and Shruti Thakur. Variable chaplygin gas: Constraints from supernovae, bao, look back time, and grbs. 2019.

Bruce Allen and Joseph D Romano. Detecting a stochastic background of gravitational radiation: Signal processing strategies and sensitivities. 1997.

H. B. Benaoum. Modified chaplygin gas cosmology. *Advances in High Energy Physics*, 2012, 2012. doi: 10.1155/2012/357802.

Kipp Cannon and Sarah Caudill et al. Gstlal: A software framework for gravitational wave discovery. *SoftwareX*, 14: 100680, 6 2021. ISSN 2352-7110. doi: 10.1016/J.SOFTX.2021.100680.

Guadalupe Cañas-Herrera, Omar Contigiani, and Valeri Vardanyan. Learning how to surf: Reconstructing the propagation and origin of gravitational waves with gaussian processes. 5 2021.

Marco Celoria, Roberto Oliveri, Alberto Sesana, and Michela Mapelli. Lecture notes on black hole binary astrophysics. 7 2018.

S Chatterji, L Blackburn, G Martin, and E Katsavounidis. Multiresolution techniques for the detection of gravitational-wave bursts. *Classical and Quantum Gravity*, 21, 10 2004. ISSN 0264-9381. doi: 10.1088/0264-9381/21/20/024.

Hsin-Yu Chen, Maya Fishbach, and Daniel E Holz. A 2 per cent hubble constant measurement from standard sirens within 5 years. 2018.

Ujjal Debnath. Gravitational waves for some dark energy models in frw universe. *Physics of the Dark Universe*, 32, 5 2021. ISSN 22126864. doi: 10.1016/j.dark.2021.100832.

B.P. Abbott et al. The basic physics of the binary black hole merger gw150914. *Annalen der Physik*, 529, 1 2017. ISSN 15213889. doi: 10.1002/andp.201600209.

B.P. Abbott et al. Properties of the binary black hole merger gw150914. *Physical Review Letters*, 116, 6 2016. doi: 10.1103/PHYSREVLETT.116.241102.

B.P. Abbott et al. Gw190425: Observation of a compact binary coalescence with total mass 3.4 m . *The Astrophysical Journal*, 892:L3, 3 2020. doi: 10.3847/2041-8213/AB75F5.

P. B. Covas et al. Identification and mitigation of narrow spectral artifacts that degrade searches for persistent gravitational waves in the first two observing runs of advanced ligo. *Physical Review D*, 97, 4 2018. doi: 10.1103/PHYSREVD.97.082002.

S. Perlmutter et al. Measurements of omega and lambda from 42 high-redshift supernovae. *The Astrophysical Journal*, 517:565–586, 12 1998. doi: 10.1086/307221.

J C Fabris, S V B Gonçalves, M S Santos, and Av Fernando Ferrari. Gravitational waves in the generalized chaplygin gas model. 2004.

Will M Farr, Maya Fishbach, Jiani Ye, and Daniel E Holz. A future percent-level measurement of the hubble expansion at redshift 0.8 with advanced ligo. 2019. doi: 10.3847/2041-8213/ab4284.

V M C Ferreira and P P Avelino. Extended family of generalized chaplygin gas models. 2018.

V Gorini, A Kamenshchik, U Moschella, V Pasquier, and L D Landau. The chaplygin gas as a model for dark energy. 2004.

Zong-Kuan Guo and Yuan-Zhong Zhang. Cosmology with a variable chaplygin gas. 2007.

Daniel E. Holz, Scott A. Hughes, and Bernard F. Schutz. Measuring cosmic distances with standard sirens. *Physics Today*, 71:34–40, 12 2018. ISSN 00319228. doi: 10.1063/PT.3.4090.

Jerry W Jensen. Supernovae light curves: An argument for a new distance modulus. 2004.

R. A. Knop and G. Aldering et al. New constraints on m , , and w from an independent set of 11 high-redshift supernovae observed with the hubble space telescope. *The Astrophysical Journal*, 598:102–137, 11 2003. doi: 10.1086/378560.

Gavin P Lamb and Shiho Kobayashi. Grb 170817a as a jet counterpart to gravitational wave trigger gw 170817. *MNRAS*, 000:1–9, 2017.

Antony Lewis and Sarah Bridle. Cosmological parameters from cmb and other data: a monte-carlo approach. 2002.

Jianbo Lu, Lixin Xu, Jiechao Li, Baorong Chang, Yuanxing Gui, and Hongya Liu. Constraints on modified chaplygin gas from recent observations and a comparison of its status with other models. *Physics Letters, Section B: Nuclear, Elementary Particle and High-Energy Physics*, 662:87–91, 4 2010. doi: 10.1016/j.physletb.2008.03.005.

Duncan M. Macleod, Joseph S. Areeda, Scott B. Coughlin, Thomas J. Massinger, and Alexander L. Urban. Gwpy: A python package for gravitational-wave astrophysics. *SoftwareX*, 13:100657, 1 2021. ISSN 2352-7110. doi: 10.1016/J.SOFTX.2021.100657.

Laura K Nuttall and Christopher P L Berry. Classical and quantum gravity a guide to ligo-virgo detector noise and extraction of transient gravitational-wave signals recent citations electromagnetic counterparts of gravitational-wave signals. 2020. doi: 10.1088/1361-6382/ab685e.

Ho Jung Paik. Sogro (superconducting omni-directional gravitational radiation observatory). volume 168. EDP Sciences, 1 2018. doi: 10.1051/epjconf/201816801005.

John A Peacock. *Cosmological physics by John A Peacock (z-lib.org).* ISBN ISBN 978-0-521-42270-3.

P J E Peebles and Bharat Ratra. The cosmological constant and dark energy.

Matthew Pitkin, Stuart Reid, Sheila Rowan, and Jim Hough. Gravitational wave detection by interferometry (ground and space). *Living Reviews in Relativity*, 14, 12 2011. ISSN 2367-3613. doi: 10.12942/lrr-2011-5.

A S Pozanenko, P Yu Minaev, S A Grebenev, and I V Chelovekov. Observation of the second ligo/virgo event connected with binary neutron star merger s190425z in the gamma-ray range. *Astronomy Letters*, 45:768–786, 2019. doi: 10.1134/S032001081911007X.

David Radice, Viktoriya Morozova, Adam Burrows, David Vartanyan, and Hiroki Nagakura. Characterizing the gravitational wave signal from core-collapse supernovae. 2019. doi: 10.3847/2041-8213/ab191a.

Adam G. Riess and Alexei V. Filippenko et al. Observational evidence from supernovae for an accelerating universe and a cosmological constant. *The Astronomical Journal*, 116:1009–1038, 5 1998. doi: 10.1086/300499.

Adam G. Riess and Louis-Gregory Strolger et al. Type ia supernova discoveries at z>1 from the hubble space telescope: Evidence for past deceleration and constraints on dark energy evolution. *The Astrophysical Journal*, 607:665–687, 2 2004. doi: 10.1086/383612.

K. Riles. Gravitational waves: Sources, detectors and searches. *Progress in Particle and Nuclear Physics*, 68, 1 2013. ISSN 01466410. doi: 10.1016/j.ppnp.2012.08.001. read about NINJA on pge 9
GW Bursts 10.

Ryan Rubenzahl. Gravitational wave radiation by binary black holes, 2017.

Barbara Ryden. Introduction to cosmology.

Varun Sahni. The cosmological constant revisited. *Pramana - Journal of Physics*, 53:937–944, 1999. doi: 10.1007/S12043-999-0048-1.

Varun Sahni. Living with lambda. *PRAMANA c Indian Academy of Sciences*, 55:559–573, 2000.

Varun Sahni and Alexei Starobinsky. The case for a positive cosmological lambda-term.

Patricia Schmidt. Studying and modelling the complete gravitational-wave signal from precessing black hole binaries, 2014.

Geetanjali Sethi, Sushil K Singh, Pranav Kumar, and Deepak Jain. Variable chaplygin gas: Constraints from cmbr and sne ia. 2018.

N Suzuki and D Rubin et al. An early-type-hosted supernova sample *. 2011.

S. A. Usman, J. C. Mills, and S. Fairhurst. Constraining the inclinations of binary mergers from gravitational-wave observations. *The Astrophysical Journal*, 877:82, 5 2019. doi: 10.3847/1538-4357/AB0B3E.

Sergiy S Vasylyev and Alexei V Filippenko. A measurement of the hubble constant using gravitational waves from the binary merger gw190814.